An attempt to link suspended load hysteresis patterns and sediment sources configuration in alpine catchments

C. Misset, A. Recking, C. Legout, A. Poirel, M. Cazilhac, M. Esteves, M. Bertrand

AN ATTEMPT TO LINK SUSPENDED LOAD HYSTERESIS PATTERNS AND SEDIMENT SOURCES CONFIGURATION IN ALPINE CATCHMENTS

Authors

C. Misset[1]*, A. Recking[1], C. Legout[2], A. Poirel[3], M. Cazihlac[3], M. Esteves[2], M. Bertrand[1].

[1] Univ. Grenoble Alpes, Irstea, ETNA, 38000 Grenoble, France

[2] Univ. Grenoble Alpes, CNRS, IRD, Grenoble INP, IGE, 38000 Grenoble, France

[3] EDF, DTG, 38100 Grenoble, France

* Corresponding author

ABSTRACT

A large part of total solid flux is transported as suspension in mountainous rivers. It is crucial for water resource management and for environmental issues to be able to model and to understand these fluxes. However, suspended load is known to be highly variable in time and space, as fine sediments can originate from various erosion processes and from various sources. Among the different methodologies available for analyzing the suspended sediment flux dynamics, hysteretic loops in discharge and suspended load signals are commonly used to assess sediment sources and production processes. However, the shape of these loops is often analyzed qualitatively for a single or a small number of catchments. Hence it is still unclear how the geomorphological catchment properties influence the variability of the flow rate - suspended sediment concentration relationship through the hysteresis effects. This is particularly true in mountainous catchments where important sources of fine sediments may originate from the river bed in addition to hillslopes.

In this study we analyzed quantitatively ten long-term series of high-frequency observations of suspended sediment load measured in contrasted alpine catchments. Hysteresis effects were analyzed in a high number of automated sampled events and the dominant response for each catchment was sought. This was done by using a normalized hysteresis index developed by Lloyd et al. (2016), which we weighted by the mass transported during each event. The various catchments were characterized with a normalized geomorphological index expressing the relative importance of sediment sources originating from the river bed or from eroded areas as a function of the distance to the outlet of the catchment.

The dominant hysteresis response of the ten alpine catchments studied was found to be greatly linked to their geomorphological index. These results suggest that the sediment source configuration upstream of a measuring station drive hysteresis effects and thus the variability of the flow rate-suspended sediment concentration relationship.

Keywords: Suspended load, hysteresis, sediment sources, alpine catchments

1. INTRODUCTION

Suspended sediment load (SSL) assessment is essential for water resource management and for many environmental issues. Whereas fine sediments transported by rivers are a vector of nutrients that are essential for estuarine ecosystems [*Le Pape et al.*, 2013; *Ludwig and Probst*, 1998], they are also associated with socio-economic issues due to reservoir siltation or contaminant transport [*Vercruysse et al.*, 2017; *Walling et al.*, 2003].

SSL is known to be highly variable in time and space especially in mountainous areas given that fine sediments can originate either from the main fluvial system or from external sources in similar proportions [*Guillon et al.*, 2018; *Navratil et al.*, 2010; *Orwin and Smart*, 2004]. According to the concept proposed by Bogen (1980) and the conceptual models used by Picouet (2009) or Park and Hunt (2017), the first type of production consists of sediment resuspension from the river bed. This part of suspension is believed to be related to flow rate, shear stress, or stream power [*Park and Hunt*, 2017]. In this case, fine sediments are produced by resuspension of deposited fine particles on bars, in secondary channels, when the armor layer is mobilized [*Navratil et al.*, 2010] or when bank erosion occurs [*Lefrançois et al.*, 2007]. The second type concerns erosion processes that take place in the catchment and that may not be directly related to the flow rate measured in the main channel. Fine particles are produced by rainfall or runoff detachment on eroded areas, in first-order tributaries or by mass movement.

The coexistence of these two kinds of fine sediment production processes often generates a huge variability in the flow rate (Q)–suspended sediment concentration (SSC) relationship. As observed in many field studies at the event, inter-event, or seasonal time scale, the same flow solicitation does not lead to the same sediment response of the watershed [*Aich et al.*, 2014; *Andermann et al.*, 2012; *Mao and Carrillo*, 2016; *Sun et al.*, 2016]. This non-unique relation between Q and SSC is often highlighted through hysteresis loop observations. These phenomena have been widely analyzed in the past few decades and in various environments [*Aguilera and Melack*, 2018; *Baca*, 2010; *Bogen*, 1980; *Gharari and Razavi*, 2018; *Klein*, 1984; *Smith and Dragovich*, 2009; *Tananaev*, 2015; *Zuecco et al.*, 2016]. The first classification of hysteresis loops was proposed by Williams (1989). Five classes were distinguished: single-valued line, clockwise loops, counterclockwise loops, single line plus a loop, and figure-of-eight loop. This classification was then re-used and completed with more complex figures by various authors such as Nistor and Church (2005), Tananaev (2015), Duvert *et al.* (2010) or Hamshaw *et al.* (2018). In a literature review, Gellis (2013) highlights that a given hysteresis effect observed at a measuring station can be explained by various erosion and physical processes.

However, at the event scale, distant sediment sources were found to generate mainly counterclockwise loops [*Baca*, 2010; *Klein*, 1984; *Williams*, 1989]. Suspended sediments are transported more or less at the mean flow velocity, which is lower than the flood wave celerity. This means that if the travelling distance and the relative difference between the celerity of the two waves is high enough, a time delay will be observed between the two signals generating a counterclockwise loop [*Klein*, 1984;

Nistor and Church, 2005; *Williams*, 1989]. By contrast, depletion in the SSC during the falling limb of the flood or an SSC peak prior to a Q peak will generate a clockwise loop. This is usually attributed to a mobilization of relatively close and supply limited sources [*Marttila and Kløve*, 2010; *Park and Hunt*, 2017], dilution due to base flow increase during the falling limb [*Baca*, 2010], or rainfall close to the catchment outlet [*Jansson*, 2002]. Many other processes could generate hysteresis between SSC and Q such as the contribution of upstream tributaries [*Asselman*, 1999], bank erosion [*Smith and Dragovich*, 2009], or hysteresis effects in the SSC–turbidity calibration curve [*Landers and Sturm*, 2013]. In some cases, the SSC and Q curve are synchronized, leading to no hysteresis pattern. Such situations were often interpreted as an unlimited sediment supply [*Nistor and Church*, 2005; *Williams*, 1989]. Finally, complex patterns can be observed for multi-peak events or when several processes described previously occur at the same time in the catchment.

Given the high number of processes leading to Q–SSC hysteresis, it is doubtful to infer even qualitatively the major erosion processes acting in a unique catchment with this single information especially when measurements are conducted for short time periods [*Esteves et al.*, 2018]. On the other hand, using measurements made on several contrasted watersheds at regional scale could help to assess to which extent the sediment sources configuration may control the shape of these hysteresis and thus to better understand the spatial variability in the Q–SSC relation. During the last decades, there has been a growing interest in sediment sources characterization [*Parsons et al.*, 2015; *Wohl*, 2017] as sediment contributing areas have been shown to control sediment yield in alpine catchments [*de Vente et al.*, 2006; *Haas et al.*, 2011]. Despite the respective contribution of each sediment sources are often highly variable in time and space [*Legout et al.*, 2013], several methods have been proposed to quantify sediment connectivity in catchments [*Borselli et al.*, 2008; *Heckmann et al.*, 2018; *Heckmann and Schwanghart*, 2013]. Most of these methods conceptually consider an upslope (contributing area) and a downslope (source to sink) component to spatially describe the capacity of the catchment to export sediments [*Borselli et al.*, 2008; *Cavalli et al.*, 2013; *Heckmann and Schwanghart*, 2013]. While this separation in two components in connectivity indexes (i.e. upslope and downslope) is similar to the conceptual distinction in two sediment sources (hillslope vs riverbed production) often depicted as the main controlling factor of discharge-suspended sediment concentration hysteresis, no study reported any attempt to quantify the potential links between hysteresis and conceptual description of sediment sources.

This study attempts to fill this gap by analyzing long-term series with high-frequency observations of SSL made in ten contrasted mountainous catchments in the French Alps. The main objectives were (i) to describe the dominant hysteresis patterns, (ii) to propose a method describing fine sediment source configuration at the catchment scale, and (iii) to analyze the link between dominant hysteresis patterns and sediment source configuration.

2. MATERIAL AND METHODS

2.1. HYDRO-GEOMORPHOLOGICAL CHARACTERISTICS OF THE CATCHMENTS

Four of the ten catchments studied (Asse, Bléone, Galabre, and Bès) are located in the southern part of the French Alps, and four others (Romanche, Arvan, Glandon, and Arc) are in the northern part (Figure 1). Two basins (Drac and Buëch) have intermediate positions. The ten catchments belong to the long-term observatory networks of two French research infrastructures (OZCAR and RZA) or from the monitoring network of Electricité de France Company (EDF).

Figure 1

2.1.1. Spatial information used

Data were collected for several characteristics of the basins (Table 1). Monthly average specific discharges were obtained from the French hydrometric agency (Banque Hydro: http://www.hydro.eaufrance.fr/) whereas spatial catchment properties were obtained thanks to a GIS analysis of several spatial databases (BD ORTHO®, BD ALTI®, Corine Land Cover®, GeoFLA®, IGN©). Active channel widths were digitalized manually on aerial orthophotographies and the fluvial corridor tool box [*Roux et al.*, 2015] was used in ARCGIS 10.3 to extract the active channel width at a regular step of 20 m. The median active river bed width calculated over the first 10 km upstream the station (W_{10}). The mean riverbed slope was obtained from the French National Institute of Geography website (https://geodesie.ign.fr/fiches/) for approximately 10 km upstream of each measuring station (S_{10}). A georeferenced dataset of polygonal features with the location of eroded areas in the Alps (https://journals.openedition.org/rga/3543#tocto2n6) was used for the Bléone, Asse, Bès, Galabre, Buëch, Drac, and Romanche catchments [*Bertrand*, 2014; *Bertrand et al.*, 2017]. These areas can be easily recognized in alpine catchments on high-resolution orthophotos and manually digitized using classic GIS toolkits or using automatic extraction procedure as it have been done in several previous studies [*Marden et al.*, 2005; *Trustrum and Stephens*, 1981; *Vrieling*, 2006]. Bertrand et al. (2017) obtained the eroded patches map used in this study by combining object-based supervised classification models on infrared aerial orthophotographies (831 tiles, 0.5 m resolution) and a pixel-based supervised classification model on Landsat 7 ETM+ images (three images, with 30 m resolution and offering a wider spectral range than aerial orthophotographies) to extract eroded areas in the southern part of the Alps. The training and validation datasets used are each constituted of 30 infrared aerial orthophotographies tiles (randomly sampled in the 831 tiles) automatically segmented into objects having homogeneous textures and manually classified into two categories: eroded areas and non-eroded areas. The final classification model is a weighted sum of these calibrated models (both object-based and pixel-based). They obtained a model sensitivity, specificity and overall classification score of respectively 0.81, 0.94 and 0.9. They also performed an expert classification on 500 randomly distributed points in the Bléone catchment and obtained similar results (0.74, 0.99 and 0.96 respectively) confirming the reliability of this method. For the Glandon, Arvan, and Arc basins, this map was not available and eroded areas were digitalized manually using 50-cm resolution aerial orthophotographies. In both cases, eroded patches are considered through the image analysis as exposed and unvegetated areas exhibiting erosion patterns or gullies. This eroded areas description is consistent with the fact that increasing bare soils cover increases suspended sediment yield [*Douglas*, 1967; *Duvert et al.*, 2012].

2.1.2. Hydrological regimes

Table 1 shows the contrasting characteristics of the ten catchments. Their areas range from 22 km² to nearly 900 km². The hydrology of the catchments located in the Southern Alps, including the Buëch basin, exhibits a high-flow period in winter and late autumn, separated by a low-flow period in summer (Figure 2). The northern catchments have higher specific water discharges. They are characterized by the presence of snow cover and glaciers resulting in a melting season generating high flows from late spring to mid-summer and low-flow periods the rest of the time. The Drac catchment exhibits an intermediate discharge regime with a melting season in late spring followed by low-flow period in summer and another high-flow period in autumn due to widespread rainfall events. The northern catchments are higher in altitude (61% of mean area above 2,000 m) than southern ones (98% of mean area under 2,000 m), with the Drac exhibiting an intermediate situation (35% of catchment area above 2,000 m).

2.1.3. Geomorphological characteristics

Various land cover and lithologies are present on these catchments. Northern catchments, including the Drac basin, have large areas prone to erosion with zones having no or low vegetation cover ranging from 24% to 51% of their total area and rocks considered as non-resistant covering between 57% and 99% of their area. The Arvan, Glandon and Romanche catchments comprise mainly narrow mountain valleys with laterally constrained streams. Few alluvial reaches are included in the dominant step-pool sections with mean river bed slopes on the first 10 km upstream the station (S_{10}) comprised between 4% and 5.9% and median river bed active widths on the first 10 km upstream the station (W_{10}) ranging between 8m and 22m. Having a larger catchment area, the Arc has a gentler river bed slope (S_{10}=1.12%) and a wider river bed active width (W_{10}=33m). It exhibits mainly plan bed sections with few gavel bars downstream active tributaries punctuated with narrow gorge sections. The Drac basin has poorly laterally constrained streams in its downstream part and a gentle slope (S_{10}=1.01%) enabling the development of braiding sections on dozen of kilometers (W_{10}=60m). Southern catchments, including the Buëch basin are also prone to erosion with a fraction of their basin that has low or no vegetation cover ranging between 10% and 19% and non-resistant rocks cover ranging between 79% and 100%. Their valleys are wider than the northern catchments except for the Galabre catchment which is a small headwater stream (A=22km^2) with constrained gorges and step-pool sections (W_{10}=8m, S_{10}=8.8%). The Bléone and Buëch exhibit braiding morphologies (W_{10} of respectively 162m and 118m) with gentle slopes (S_{10} of respectively 0.82% and 0.81%). The Asse and Bès catchments also exhibit long alluvial and gentle sections which are punctuated with narrower sections in gorges or more constrained valleys (W_{10} of respectively 28m and 20m, S_{10} of respectively 0.87% and 2.57%). Mano *et al.* (2009) reported specific suspended sediment fluxes around 500 t km^{-2} year^{-1} for the Asse, Bléone and Romanche catchment while Navratil *et al.* (2012) reported specific suspended sediment fluxes of respectively 330, 690, and 680 t km^{-2} year^{-1} for the Bléone, Bès and Galabre basins which can be classified as high according to the classification proposed by Meybec *et al.* (2003). These studies suggest that the studied catchments have highly active fine sediment sources. Also, all of these catchments have been chosen for their limited human impact, i.e. with limited presence of embankments or weirs in the rivers, limited urbanized areas and absence of large dams. Few small water intakes with limited storage capacity are however present (Glandon, Arvan, Drac, Romanche and Arc basins) but can be considered to have a negligible effect on the downstream suspended load transfer during the studied flood events.

Figure 2

Table 1

2.2. SUSPENDED LOAD TIME SERIES

The available SSL time series range from 3 to 10 years (Table 1). For each catchment, the water discharges Q were calculated from automated measurements of the water levels with a frequency of 1 h. Stage-discharge rating curves were obtained thanks to numerous technics (Acoustic Doppler Current Profiler, salt-dilution, current meters or Large Scale Particle Image Velocimetry techniques), regularly performed during the study period. The surrogate technique for SSC estimation (i.e., turbidity-meter), coupled with direct sampling of SSC for calibration was used as commonly done for such field monitoring [*Mano et al.*, 2009; *Navratil et al.*, 2011]. SSC was assumed to be uniform over the cross section owing to the high levels of turbulence in these rivers, generating well-mixed flows. SSL was computed by multiplying SSC and Q at a 1-h frequency.

2.3. HYSTERESIS ANALYSIS TOOLS

In order to determine the dominant hysteresis pattern for the ten alpine catchments, a database of runoff events was created. Individual events were selected considering both SSL and SSC. In a first step, the events having a maximum SSL below a given threshold were not considered. A SSL threshold value ($SSL_{1\%}$) was used, corresponding to the value below which 1% of the cumulated suspended sediment fluxes were transported (Figure 3). A similar approach was adopted to remove events exhibiting

SSC values below a threshold corresponding to 1% of the cumulated suspended sediment fluxes ($SSC_{1\%}$).

Figure 3

The normalized index (HI_{Lloyd}) proposed by Lloyd et al. (2016) was used (Eq. 3). This non-dimensional index is non-sensitive to the absolute value of SSC and Q, which makes it possible to do inter-event and inter-catchment comparison of hysteresis strength and direction. This index tends towards +1 for clockwise loops and towards -1 for counterclockwise loops.

To compute HI_{Lloyd} for a given event, SSC and Q were normalized using their minimum and maximum values (Eq. 1 and Eq. 2) to obtain SSC* and Q*. The differences between SSC* monitored during the rising and the falling limb were then computed for each of the 100 values of Q* ranging between 0.01 and 1 (Figure 4). Finally, HI_{Lloyd} corresponds to the mean of these differences (Eq. 3).

Figure 4

$$SSC_i{}^* = \frac{SSC_i - SSC_{min}}{SSC_{max} - SSC_{min}} \tag{1}$$

$$Q_i{}^* = \frac{Q_i - Q_{min}}{Q_{max} - Q_{min}} \tag{2}$$

$$HI_{Lloyd} = mean\left[SSC_i{}^*{}_{rising}(Q_i{}^*) - SSC_i{}^*{}_{falling}(Q_i{}^*)\right]$$

$$i \in [0.01,1] \tag{3}$$

For each catchment and each selected events, a HI_{Lloyd} value was calculated. The median value was considered representative of the dominant hysteresis patterns $(median(HI_{Lloyd}))$. However, the most frequent hysteresis patterns might not necessarily be those that transport most of the fine sediments. Thus, a new index (HI_{Ms}) was introduced to investigate the "transport efficiency" associated to hysteresis. This was achieved by weighting each event by the transported mass (Ms_i):

$$HI_{Ms} = \frac{\sum(HI_{Lloyd_i} \times Ms_i)}{\sum Ms_i} \tag{4}$$

Whereas several HI_{Lloyd} index are calculated (one for each event), only one HI_{MS} index is calculated (for the series of events) and inform which HI_{Lloyd} index is associated with the maximum transport.

These two continuous indexes were completed with classic pattern classifications [*Gellis*, 2013; *Williams*, 1989]. Hysteresis patterns were arbitrarily considered as clockwise when at least 80% of positive differences were observed between SSC^* during the rising and falling limb (Nb_{cl}). Counterclockwise loops were considered when at least 80% of negative differences were obtained (Nb_{ccl}). Otherwise, the flood was considered to have a complex hysteresis patterns or no hysteresis $(Nb_{complex})$. Finally, the percentages of the mass transported as clockwise hysteresis (Ms_{cl}), as counterclockwise hysteresis (Ms_{ccl}), and as complex or no hysteresis $(Ms_{complex})$ were calculated for each catchment. This classification permits a direct comparison between the number of events having a certain shape and the mass exported within this shape.

2.4. SEDIMENT SOURCES CHARACTERIZATION

Figure 5

An analysis of each catchment was performed following the conceptual sediment sources description (river bed vs hillslopes) proposed by Bogen (1980) and often considered for qualitative hysteresis interpretations at the catchment scale [*Buendia et al.*, 2016; *Guillon et al.*, 2018; *Mao and Carrillo*, 2016; *Smith and Dragovich*, 2009]. According to connectivity concepts developed by Borselli *et al.* (2008) and Cavalli *et al.* (2013), the area of eroded patches and the traveling distance needed to reach the outlet from these zones are important factors controlling the catchment connectivity. Also, according to numerous studies on fine sediments storage in the river network, the river width and the rived bed area are parameters that have a strong control on the quantity of fine particles that can be stored in the river bed [*Collins and Walling*, 2007; *Lambert and Walling*, 1988; *Navratil et al.*, 2010; *Piqué et al.*, 2014]. These latter parameters may also be good proxies of the buffering capacity of the river bed and of its influence on fine sediments connectivity. Indeed, the exchanging surface between the flow and the river bed may have important control on fine particles infiltration in the gravel matrix [*Frostick et al.*, 1984; *Mooneyham and Strom*, 2018].

Following these evidences, a simplified sediment sources characterization was developed. The surface occupied by the active river channel width was considered as the first type of sediment source, whereas eroded areas were considered as the second type (Figure 5). The erosion maps described in section 2.1 were used for eroded areas identification. The distance needed by the water to reach the measuring station for each of these eroded area was estimated by using a digital elevation model with 25-m horizontal resolution and various algorithms of the Spatial Analyst toolbox of ARCGIS

10.3 (Fill, FlowLength, and FlowDirection). This water path from eroded areas to the outlet of the basin was calculated by considering the maximum slope for each grid of the digital elevation model. For a given location in the watershed, and considering the total area between this point and the measuring station downstream, we defined the cumulative eroded area as the sum of the eroded patches area ($A_{eroded\ cum}$) and the cumulative area of the river bed as the sum of the active channel area ($A_{bed\ cum}$), which was extracted using the active channel width digitalization. These two cumulative areas as well as their ratio ($A_{eroded\ cum}/A_{bed\ cum}$) were calculated for each distance *x* from the monitoring station, with an incremental spatial step of 20 m, from downstream to upstream. For each catchment, the most upstream point was arbitrarily defined by a drainage area threshold of 1 km². This point was located at a flow distance L from the outlet. Finally, the Sources Configuration Index (SCI_x) was defined as the mean of the ratios ($A_{eroded\ cum}/A_{bed\ cum}$) calculated for the first x percent of the distance L:

$$SCI_x = mean\left(\frac{A_{eroded\ cum}\,(i)}{A_{bed\ cum}\,(i)}\right), i \in [0\,;x] \tag{5}$$

This geomorphological index gives information on the relative importance of each type of sediment source depending on the distance from the measuring station. It is a simplified description developed to test the reliability of usual qualitative interpretation made for hysteresis patterns (hillslopes vs river bed). The slope is not explicitly taken into account even if it is often negatively correlated with the active river width. Likewise, local weighting factors (roughness or land use in Borselli *et al.* (2008) and Cavalli *et al.* (2013)) that could better describe the capacity to produce, transfer or store fine sediments were not considered as they were difficult to estimate “a posteriori” and more questionable for suspended load than for bedload or debris flow processes.

This simple index permits to compare different spatial sources configuration (Figure 6). For instance, simplified conceptual cases (a) and (b) could probably lead to different hysteresis patterns at the outlet of the basin even if they have similar total cumulated bed and eroded area at the catchment scale. In case (a), eroded areas are located in the upper part of the basin whereas large storage zones of the river bed are located in the downstream part close to the monitoring station. Case (b) has the same bed configuration but eroded areas are located much closer to the outlet of the catchment ($d_1 >> d_2$). In that case, the ratio ($A_{eroded\ cum}/A_{bed\ cum}$) increases much closer to the outlet than in case (a). Calculating the mean value of this ratio on a given distance permits to discriminate between these two cases. They have the same $A_{eroded\ cum}/A_{bed\ cum}$ ratio considering the total length (x=100%), but the mean of these ratios calculated for x between 0% and 100% (SCI_{100} , average of the red curve in Figure 6) is much lower in case (a) than in case (b). Comparing conceptual cases (a) and (c) highlights the capacity of the index to compare different buffering effect played by the river bed. These cases have similar eroded areas located at the same distance from outlet (d_1) but the cumulative bed area is much lower in case (c). Eroded areas could be less buffered in case (c) than in case (a). The mean value of the $A_{eroded\ cum}/A_{bed\ cum}$ ratio calculated for x between 0% and 100% (SCI_{100}) will be smaller in case (a) than in case (c).

Figure 6

In order to discriminate the relative influence of hillslope sources and river bed on the hysteresis variability, an Eroded Area Index (EAI_x) and a Bed Area Index (BAI_x) were also defined and calculated for the ten catchments (Eq. 6 and Eq. 7).

$$EAI_x = \frac{mean(A_{eroded\ cum}\,(i))}{\max(A_{eroded\ cum}\,)}, i \in [0\,;x] \quad (6)$$

$$BAI_x = \frac{mean(A_{bed\ cum}\,(i))}{\max(A_{bed\ cum}\,)}, i \in [0\,;x] \quad (7)$$

3. RESULTS

3.1. RUNOFF EVENT CHARACTERISTICS

Following the event selection procedure (see Figure 3), the thresholds for SSL and SSC were calculated, and a dataset of events was created for each river (Table 2). More events were selected for northern catchments exhibiting daily floods during the melting season. While the observation periods were similar for the Glandon and the Asse, there were twice more selected events for the Glandon. Large differences were also observed in $SSL_{1\%}$ and $SSC_{1\%}$ values, e.g., the Galabre and the Bès rivers have suspended fluxes transported for higher values of SSC in comparison with other rivers.

Table 2

3.2. VARIABILITY OF DISCHARGE-CONCENTRATION HYSTERESIS IN ALPINE CATCHMENTS

While the standard deviations of the HI_{Lloyd} were rather high for all catchments, some consistent observations can be made on the basis of the median HI_{Lloyd} (Table3, Figure 7). Most rivers exhibited median values of HI_{Lloyd} around zero, because this value was often the most frequent and also because high positive or negative values had similar frequencies. This suggests an absence of a dominant hysteresis trend (clockwise or counterclockwise) in terms of the frequency of events having a certain shape. However, mainly clockwise loops (median(HI_{Lloyd})>>0) were observed for the Buech, Drac, and Bléone catchments that have dominant braided bed morphology close to the monitoring stations, suggesting a more frequent contribution of the river bed sediment sources than in other catchments.

Different conclusions can be drawn when comparing the HI_{MS} index (most transporting) with the median (most frequent) HI_{Lloyd} index for each catchment (Table 3 and Figure 7). In northern catchments, median HI_{Lloyd} and $\mathrm{HI}_{\mathrm{Ms}}$ values were similar (maximum index difference of 0.02). However in the soutern catchments, larger differences were observed between the two hysteresis indexes with differences (median(HI_{Lloyd}) minus $\mathrm{HI}_{\mathrm{Ms}}$) ranging between -0.13 and +0.16. Thus, the most frequent hysteresis shape was often not the most transport efficient one. For instance, 23% of events were classified as clockwise in the Asse and they contribute to 58% of the total SSL while 31% of events were classified as counterclockwise and contribute to only 11% of the total SSL. This suggests a higher transport efficiency of clockwise hysteresis patterns than counterclockwise ones.

Table 3

Figure 7

3.3. SEDIMENT SOURCES ANALYSIS

Large differences in the relative location of river bed and eroded area sediment sources were observed between catchments. As shown in Figure 8b, the Arvan exhibited large eroded areas close to the measuring station with a limited bed area leading to a ratio of $A_{eroded\ cum}/A_{bed\ cum}$ equal to one at a distance of roughly 7 km. By contrast, for the Bléone, the bed area is larger than the eroded areas in the first 50 km close to the monitoring station (Figure 8-a). The cumulative eroded areas exceeded the cumulative bed areas only after 55 km.

Figure 8

To quantitatively compare these differences between the ten basins we plot in Figure 9:

- $\frac{A_{eroded\ cum}(x)}{\max(A_{eroded\ cum})}$: the fraction of the total cumulative eroded area as a function of the distance from the outlet,
- $\frac{A_{bed\ cum}(x)}{\max(A_{bed\ cum})}$: the fraction of the total cumulative bed area as a function of the distance from the outlet,
- SCI_x: the average values of the ratios $A_{eroded\ cum}/A_{bed\ cum}$ calculated on a given distance upstream the outlet (0% to x%).

For the ten catchments, the cumulative bed area exhibited a relative constant increase with increasing distance to the outlet (Figure 9-a). This suggests that bed areas were, as a first approximation, homogeneously distributed along the x distance. In comparison, the cumulative eroded area showed a more sudden increase with the increasing distance to the outlet (Figure 9-b). A small fraction of eroded area was located close to the monitoring stations as less than 50% of eroded areas are located for x distance smaller than 0.5 and less than 10% for x smaller than 0.2. Also, much more variability between the ten catchments was observed. For instance, the normalized cumulative eroded area of the Romanche basin starts to increase significantly for x around 0.5 while the Bléone basin showed a sudden increase for x larger than 0.8. This suggests that eroded areas were located more in the upstream part of the Bléone watershed than for the Romanche. Some catchments as the Arc basin exhibited a more smooth increase indicating a more homogeneous eroded patches distribution along the x distance.

Finally, the source configuration index SCI_x (Eq.5) shows for all rivers an increase in the relative importance of eroded areas as compared with bed areas when moving in the upstream direction (Figure 9-c). This confirms that river bed sources were closer to the measuring station than eroded areas sources. However, some small eroded tributaries could locally generate a high value of SCI_x near the observation station, as was the case for the Galabre River. SCI_x were highly variable from one catchment to another. The shortest distance considered (*x*=10 %) to compute this index led to small differences between catchments whereas longer distances led to large differences. For instance, the two extreme cases, the Bléone and Arvan rivers, had the same SCI_{10} (0.1) but their SCI_{100} values were very different (0.3 and 21.3, respectively). The sources indexes (SCI_x, BAI_x, EAI_x) values calculated for x ranging from 10% to 100% with a x step of 10% are provided as supplementary material for more details.

Figure 9

3.4. RELATION BETWEEN SEDIMENT SOURCES CONFIGURATION AND DOMINANT HYSTERESIS PATTERNS

The general catchment characteristics, the index describing the river bed area distribution (BAI_x), the index describing the eroded area distribution (EAI_x) and the index comparing river bed and eroded area distribution (SCI_x) were compared with the dominant hysteresis pattern for each catchment (Table 4). While some significant correlations were found between general catchment characteristics and hysteresis indexes, the values remained rather low and did not exceed 0.63. Overall the Lloyd hysteresis index (HI_{Loyd}) exhibited only limited and small significant correlations with the three sediment sources indexes (SCI_x, BAI_x, EAI_x), in comparison with the mass weighted hysteresis index (HI_{MS}).

Significant negative correlations ($\rho < -0.98, pvalue < 0.01$) were found between HI_{MS} and the sediment sources index (SCI_x, Figure 10 and Table 4). This result suggests that the part of the fluxes exported with clockwise loops decreases when the relative importance of the eroded areas relative to the bed areas increases. Lower but also significant negative correlations ($\rho < -0.71, pvalue < 0.01$) were obtained between the mass weighted hysteresis index (HI_{MS}) and the eroded area distribution index (EAI_x) while no significant correlations were obtained between HI_{MS} and the bed area distribution index (BAI_x). It indicates that the spatial distribution of eroded areas in the catchment is an important factor for explaining the hysteresis variability while river bed area distribution alone cannot explain this variability. However using both information (i.e. bed area distribution combined with eroded area distribution, SCI_x) permits a much better explanation of the hysteresis variability between catchments than considering eroded area distribution alone.

The correlation between the mass weighted hysteresis index HI_{MS} and the sediment source configuration index SCI_x (in a lesser extent with eroded area distribution index EAI_x) was found to increase when averaging the values over increasing distance (x) from the outlet. Both explanatory variables reached their maximum correlation value at a distance upstream of the monitoring station of approximately 70% (Table 4 and Figure 10). The closest source configuration indexes were not found to explain the variability of hysteresis patterns between catchments, suggesting that close source configurations alone cannot explain the suspended load dynamics.

Table 4

Figure 10

4. DISCUSSION

4.1. DOMINANT HYSTERESIS PATTERNS AND TRANSPORT EFFICIENCY

Hysteresis effects are usually analyzed by counting the number of events having a certain shape [*Aguilera and Melack*, 2018; *Aich et al.*, 2014; *Buendia et al.*, 2016; *Hamshaw et al.*, 2018; *Navratil et al.*, 2010]. However, the comparison done in this study of ten contrasted alpine catchments highlighted that different results can be obtained by considering the fluxes transported with a given shape (Figure 7). From these results, two recommendations can be made, depending on the objective of the study. For those aiming at identifying the dominant sediment production processes for a given catchment, the hysteresis analysis should necessarily consider the intensity of each event, i.e., the average mass weighted hysteresis index. For studies aiming at understanding more in detail the hydro-sedimentary catchment functioning both in terms of occurrence and efficiency of the events transporting fine sediments, the analysis of hysteresis should be done simultaneously for both indexes. In our case, no relation was found between the median value of the Lloyd hysteresis index (HI_{Lloyd}) considering the number of events and any sediment source index (SCI_x, EAI_x, BAI_x) while significant correlations were found with the average mass weighted index. This suggests that the transport efficiency of hysteresis loops should be considered as a proxy of sediment production processes.

Calculating the two indices also allowed us to observe distinct behaviors for the ten alpine catchments. The differences between the fluxes exported and the frequency of events having a certain hysteresis shape were much higher for the southern catchments including the Buëch River than for the northern ones (Figure 7). This could be due to differences in hydrological regimes (Figure 2). Indeed, the southern catchments exhibited a more pronounced seasonal variability of the hysteresis values than the northern ones (Figure 11). Counterclockwise patterns were mainly observed during summer, corresponding to dry periods associated to short and intense convective storms. Clockwise patterns were observed during wet periods characterized by low intensity but rather long precipitation events leading to larger rainfall amounts than during summer. These results were consistent with those from Navratil et al. (2012) reporting that clockwise hysteresis loops exported the bulk of total suspended load during widespread flood events in the Bléone catchment. They observed marked counterclockwise loops during summer rainstorms in upper tributaries which generate suspended fluxes that were not efficiently transferred downstream. This might explain why large differences were observed between the frequency and the fluxes exported with a given hysteresis for these southern basins. Similar trends were observed by Soler *et al.* (2008) or Buendia *et al.* (2016) in Pyrenean catchments having similar hydrological regimes. In comparison, the northern catchments exhibited a much more constant export of fine sediments during the frequent daily flood events of the melting season. Many more flood events were observed for similar monitoring periods in the north than in the south (Table 2). Mano et al. (2009) reported that 90% of the suspended fluxes were transported in 5% and 7% of the time for the Bléone and Asse Rivers, respectively, while 25% of the time was needed for the Romanche River.

Figure 11

4.2. INFLUENCE OF CATCHMENT GEOMORPHOLOGICAL CHARACTERISTICS

The relation between the mass weighted hysteresis and catchment sources configuration (river bed vs. eroded areas) is consistent with previous findings and typical qualitative analyses of the hysteresis patterns which considers that a counterclockwise loops indicates a distant contribution while a clockwise loop results from a relatively close source mobilization [*Bogen*, 1980; *Gellis*, 2013; *Guillon et al.*, 2018; *Mao and Carrillo*, 2016; *Navratil et al.*, 2012; *Navratil et al.*, 2010; *Smith and Dragovich*, 2009]. Influence of watershed characteristics on SSL hysteresis patterns was observed by Aguilera *et al.* (2018) in ten mountainous Californian catchments. Also, using a random forest model on 45 measuring stations, Vaughan et al. (2017) showed that considering near-channel morphological characteristics in addition to land use contributes to a better explanation of the sediment rating curve parameters than using land use only. Their random forest model explained 38% and 43% of the hysteresis variance when considering respectively only watershed metrics or watershed plus near channel metrics. In our analysis, we also observed that both sources need to be considered. However our results show the importance to consider not only global catchments properties but the relative importance of these two types of sources (bed vs eroded areas) as well as their "travelling distance" to the monitoring station to explain hysteresis variability between catchments. Also, as was observed by Vaughan et al. (2017), we should stress that including the bed area information by considering the relative spatial distribution of eroded versus bed area (SCI_x) and not the spatial distribution of eroded area (EAI_x) alone, permits a much better explanation of the hysteresis variability and thus of the suspended load dynamics. This result is also consistent with several studies that reported a significant buffering effect played by the river bed which could be considered as a significant fine sediment source in mountainous catchments having relatively large and active alluvial reaches [*Guillon et al.*, 2018; *Navratil et al.*, 2012; *Navratil et al.*, 2010; *Orwin and Smart*, 2004].

The results obtained in this paper and in previous studies bring us to propose the following conceptual description of hysteresis and sediment configuration interactions (Figure 12). The dominant hysteresis effect observed at a given location in a catchment could depend on the upstream capacity to produce distant erosion and to buffer these upstream fluxes. If the remobilization of fine sediments from the river bed did not exist, mainly counterclockwise hysteresis should have been observed because of celerity differences between the flow rate and SSC waves [*Klein*, 1984]. Thus, the hysteresis patterns would depend on the location of the observation point for a given geomorphological scale (point A, B, C or D in Figure 12). Following the conceptual configuration in Figure 12, the fraction of SSL coming from the river bed and driven by the total flow rate could increase when moving to the downstream part of a catchment, while SSL coming directly from primary hillslope sources and driven by rainfall or runoff could decrease. Such scale dependencies of hysteresis processes have been already noticed in hydrological studies [*Gharari and Razavi*, 2018]. For instance, Davies and Beven (2015) have shown by using a synthetic case that hysteresis between streamflow and catchment storage was changing with the catchment size considered.

Figure 12

4.3. LIMITATIONS AND IMPLICATIONS

Given the wide range of characteristics of the 10 studied alpine catchments, comprising various sizes, geologies, altitudes, hydrological and sedimentary regimes the proposed approach can be considered as relevant in other mountainous environments. However, its relevance should be tested in other contexts such as low-land, agricultural or arid environments. The analysis of the sediment sources might be improved to get a more detailed description of the catchment sources configuration to investigate its relation with suspended load at shorter spatial and temporal scales. For instance, the mechanical properties of rocks in eroded areas could be taken into account to give more importance to soft rocks than to more resistant ones for catchments with contrasted lithologies. The local river bed slope could also be explicitly considered in addition to the active river width to get a proxy of the buffering capacity of the bed. This would probably give less importance to steep streams and more importance to gentle ones. These potential improvements might be tested in future work.

However, while the approach used does not represent all the complexity of interactions between suspended load and sediment source configuration a significant part of the variability of SSL hysteresis can be explained by this simplified source description at a regional scale. This confirms the strong link between hysteresis processes and the variable sediment sources activation that have been qualitatively described for decades [*Gellis*, 2013; *Gharari and Razavi*, 2018; *Williams*, 1989]. Our results suggest that even for small catchments, fine sediment dynamics and hysteresis effects could be largely influenced by erosion and deposition processes occurring in the river bed. This might be the case in catchments where eroded areas are located far enough upstream so that the main channel can act as a buffering reservoir of fine sediments. However, larger catchments with well-developed fluvial systems could, conversely, be influenced in a non-negligible way by hillslope process production if some eroded areas are located at a short distance from the monitoring station. Both processes are probably inevitably linked. The fractions of SSL coming from the bed or from the hillslopes seem to change depending on the point considered in the catchment. The simple sediment sources analysis proposed in this study could be performed prior to the installation of a gauging station or prior to modeling effort in order to assess which kind of processes should be considered in a conceptual modeling approach. It could also be helpful to determine the dominant fine sediment production process for river or dam management at the catchment scale.

5. CONCLUSIONS

This study aimed at testing the links between Discharge-Suspended Sediment Concentrations (Q-SSC) hysteresis and the spatial configuration of sediment sources which have been qualitatively considered for decades without been quantitatively tested. A quantitative analysis of sediment sources configuration and Q–SSC hysteresis was performed in ten contrasted alpine catchments. Hysteresis indexes were calculated on a high number of automated sampled events to extract the dominant hysteresis pattern for each catchment. Simple indexes were developed to describe the river bed and eroded patches area distribution as well as a “travelling distance to the outlet”. The main findings can be summarized as follows:

(i) Considering the dominant SSL hysteresis in a given catchment as the most frequent pattern or as the most efficient in terms of transport can lead to different results. Our observations suggest that the transport efficiency of hysteresis should be considered to infer the dominant sediment production process. This could be particularly true for catchments having most of their fluxes exported during few short events and exhibiting marked seasonal hysteresis variability. Thus an averaged mass weighted hysteresis index was proposed.

(ii) A strong correlation was found between mass weighted hysteresis index and sediment sources configuration index (river bed vs eroded area) which confirms the qualitative interpretations often made for SSC-Q hysteresis processes. We also observed that the sources configuration should be considered on a long enough fraction of the catchment (at least 50% of the whole principal river network) upstream the observation point to explain the spatial hysteresis variability. This is consistent with the rather long travelled distances of suspended particles.

(iii) In comparison to previous studies, these results show the importance to consider not only general catchment properties or sediment sources to understand SSL dynamics but their spatial distribution and connectivity. Furthermore, including bed related information increases significantly the explanatory power of the SSC-Q hysteresis variability than using only primary hillslope sources information.

6. NOTATIONS

The following symbols are used in this paper.

SSL	Suspended sediment load
SSC	Suspended sediment concentration
Q	Flow rate
A	Catchment area
No	Fraction of catchment with low or no vegetation cover
Fo	Fraction of catchment forest cover
Gl	Fraction of catchment with glacier cover
SCR	Fraction of catchment with soft coherent rock cover
HR	Fraction of catchment with heterogeneous rock cover
RR	Fraction of catchment with resistant rock cover

W_{10}	Median active width extracted on the first 10 km upstream the station
S_{10}	Mean riverbed slope extracted on the first 10 km upstream the station
q	Mean annual specific discharge
HI_{Lloyd}	Lloyd hysteresis index
SSC^*	Normalized suspended sediment concentration at the flood scale
Q^*	Normalized flow rate at the flood scale
HI_{Ms}	Mass weighted average hysteresis index
Ms_i	Mass of suspended sediment transported during the event i
Nb_{cl}	Fraction of event having a clockwise hysteresis shape
Nb_{ccl}	Fraction of event having a counterclockwise hysteresis shape
$Nb_{complex}$	Fraction of event having complex or no hysteresis shape
Ms_{cl}	Fraction of the mass exported with a clockwise hysteresis shape
Ms_{ccl}	Fraction of the mass exported with a counterclockwise hysteresis shape
$Ms_{complex}$	Fraction of the mass exported with complex or no hysteresis hysteresis
$A_{eroded\ cum}$	Cumulative eroded area at a given distance from the station
$A_{bed\ cum}$	Cumulative riverbed area at a given distance from the station
SCI_x	Sources Configuration Index (mean ratio of cumulative eroded area over cumulative bed area calculated on the first x% of the main channel length)
EAI_x	Eroded Area Index (mean cumulative eroded area over total eroded area on the first x% of the main channel length)
BAI_x	Bed Area Index (mean cumulative bed area over total bed area on the first x% of the main channel length)
L	Maximum distance used to compute the sediment source configuration

	index
$SSL_{99\%}$	Threshold on SSL above which 99% of cumulated suspended fluxes are transported
$SSC_{99\%}$	Threshold on SSC above which 99% of cumulated suspended fluxes are transported
t_{exceed}	Minimum time step for which a SSL should exceed all following and preceding values for the event detection

7. ACKNOWLEDGEMENTS

This study was founded by IRSTEA (National Research Institute of Science and Technology for the Environment and Agriculture) and EDF (Electricité de France). The field monitoring data provided by IRSTEA, EDF and IGE (Institute for Geosciences and Environmental research) field teams are greatly appreciated. The authors also want to thank three anonymous reviewers who greatly contributed to improve to this paper by providing helpful reviews of an earlier version of this manuscript.

8. REFERENCES

Aguilera, R., and J. M. Melack (2018), Concentration-Discharge Responses to Storm Events in Coastal California Watersheds, *Water Resources Research*, *54*(1), 407-424, doi:10.1002/2017wr021578.

Aich, V., A. Zimmermann, and H. Elsenbeer (2014), Quantification and interpretation of suspended-sediment discharge hysteresis patterns: How much data do we need?, *Catena*, *122*, 120-129, doi:10.1016/j.catena.2014.06.020.

Andermann, C., A. Crave, R. Gloaguen, P. Davy, and S. Bonnet (2012), Connecting source and transport: Suspended sediments in the Nepal Himalayas, *Earth and Planetary Science Letters*, *351-352*, 158-170, doi:10.1016/j.epsl.2012.06.059.

Asselman, N. E. M. (1999), Suspended sediment dynamics in a large drainage basin: the River Rhine, *hydrological Processes*, *13*, 1437-1450, doi:10.1002/(SICI)1099-1085(199907)13:10<1437::AID-HYP821>3.0.CO;2-J.

Baca, P. (2010), Hysteresis effect in suspended sediment concentration in the Rybárik basin, Slovakia / Effet d'hystérèse dans la concentration des sédiments en suspension dans le bassin versant de Rybárik (Slovaquie), *Hydrological Sciences Journal*, *53*(1), 224-235, doi:10.1623/hysj.53.1.224.

Bertrand, M. (2014), PhD thesis : Debris-flow susceptibility assessment at the regional scale of the Southern French Alps, Ecole normale supérieure de lyon, <NNT : 2014ENSL0895>. <tel-01022867>.

Bertrand, M., F. Liébault, and H. Piégay (2017), Regional Scale Mapping of Debris-Flow Susceptibility in the Southern French Alps, *Revue de géographie alpine*(105-4), doi:10.4000/rga.3543.

Bogen, J. (1980), The hysteresis effect of sediment transport systems, *Norsk Geografisk Tidsskrift - Norwegian Journal of Geography*, *34*(1), 45-54, doi:10.1080/00291958008545338.

Borselli, L., P. Cassi, and D. Torri (2008), Prolegomena to sediment and flow connectivity in the landscape: A GIS and field numerical assessment, *Catena*, *75*(3), 268-277, doi:10.1016/j.catena.2008.07.006.

Buendia, C., D. Vericat, R. J. Batalla, and C. N. Gibbins (2016), Temporal Dynamics of Sediment Transport and Transient In-channel Storage in a Highly Erodible Catchment, *Land Degradation & Development*, *27*(4), 1045-1063, doi:10.1002/ldr.2348.

Cavalli, M., S. Trevisani, F. Comiti, and L. Marchi (2013), Geomorphometric assessment of spatial sediment connectivity in small Alpine catchments, *Geomorphology*, *188*, 31-41, doi:10.1016/j.geomorph.2012.05.007.

Collins, A. L., and D. E. Walling (2007), The storage and provenance of fine sediment on the channel bed of two contrasting lowland permeable catchments, UK, *River Research and Applications*, *23*(4), 429-450, doi:10.1002/rra.992.

Davies, J. A. C., and K. Beven (2015), Hysteresis and scale in catchment storage, flow and transport, *Hydrological Processes*, *29*(16), 3604-3615, doi:10.1002/hyp.10511.

de Vente, J., J. Poesen, P. Bazzoffi, A. V. Rompaey, and G. Verstraeten (2006), Predicting catchment sediment yield in Mediterranean environments: the importance of sediment sources and connectivity in Italian drainage basins, *Earth Surface Processes and Landforms*, *31*(8), 1017-1034, doi:10.1002/esp.1305.

Douglas, I. A. N. (1967), Man, Vegetation and the Sediment Yields of Rivers, *Nature*, *215*(5104), 925-928, doi:10.1038/215925a0.

Duvert, C., N. Gratiot, O. Evrard, O. Navratil, J. Nemery, C. Prat, and M. Esteves (2010), Drivers of erosion and suspended sediment transport in three headwater catchments of the Mexican Central Highlands, *Geomorphology*, *123*(3-4), 243-256, doi:10.1016/j.geomorph.2010.07.016.

Duvert, C., et al. (2012), Towards prediction of suspended sediment yield from peak discharge in small erodible mountainous catchments (0.45–22km2) of France, Mexico and Spain, *Journal of Hydrology*, *454-455*, 42-55, doi:10.1016/j.jhydrol.2012.05.048.

Esteves, M., C. Legout, O. Navartil, and O. Evrard (2018), Medium term high frequency observation of discharge and suspended sediment in a Mediterranean mountainous catchment, *Journal of Hydrology*, *Accepted*.

Frostick, L. E., P. M. Lucas, and I. Reid (1984), The infiltration of fine matrices into coarse-grained alluvial sediments and its implications for stratigraphical interpretation *Journal of the Geological Society*, *141*(6), 955-965, doi:10.1144/gsjgs.141.6.0955.

Gellis, A. C. (2013), Factors influencing storm-generated suspended-sediment concentrations and loads in four basins of contrasting land use, humid-tropical Puerto Rico, *Catena*, *104*, 39-57, doi:10.1016/j.catena.2012.10.018.

Gharari, S., and S. Razavi (2018), A review and synthesis of hysteresis in hydrology and hydrological modeling: Memory, path-dependency, or missing physics?, *Journal of Hydrology*, *566*, 500-519, doi:10.1016/j.jhydrol.2018.06.037.

Guillon, H., J.-L. Mugnier, and J.-F. Buoncristiani (2018), Proglacial sediment dynamics from daily to seasonal scales in a glaciated Alpine catchment (Bossons glacier, Mont Blanc massif, France), *Earth Surface Processes and Landforms*, *43*(7), 1478-1495, doi:10.1002/esp.4333.

Haas, F., T. Heckmann, V. Wichmann, and M. Becht (2011), Quantification and Modeling of Fluvial Bedload Discharge from Hillslope Channels in two Alpine Catchments (Bavarian Alps, Germany), *Zeitschrift für Geomorphologie, Supplementary Issues*, *55*(3), 147-168, doi:10.1127/0372-8854/2011/0055s3-0056.

Hamshaw, S. D., M. M. Dewoolkar, A. W. Schroth, B. C. Wemple, and D. M. Rizzo (2018), A New Machine-Learning Approach for Classifying Hysteresis in Suspended-Sediment Discharge Relationships Using High-Frequency Monitoring Data, *Water Resources Research*, *54*(6), 4040-4058, doi:10.1029/2017wr022238.

Heckmann, T., M. Cavalli, O. Cerdan, S. Foerster, M. Javaux, E. Lode, A. Smetanová, D. Vericat, and F. Brardinoni (2018), Indices of sediment connectivity: opportunities, challenges and limitations, *Earth-Science Reviews*, *187*, 77-108, doi:10.1016/j.earscirev.2018.08.004.

Heckmann, T., and W. Schwanghart (2013), Geomorphic coupling and sediment connectivity in an alpine catchment — Exploring sediment cascades using graph theory, *Geomorphology*, *182*, 89-103, doi:10.1016/j.geomorph.2012.10.033.

Jansson, M. B. (2002), Determining sediment source areas in a tropical river basin, Costa Rica, *Catena*, *47*, 63–84, doi:0341-8162/02/$.

Klein, M. (1984), Anti clockwise hysteresis in suspended sediment concentration during individual storms: Holbeck Catchment; Yorkshire, England, *Catena*, *11*, 251-257, doi:https://doi.org/10.1016/0341-8162(84)90014-6.

Lambert, C. P., and D. E. Walling (1988), Measurement of Channel Storage of Suspended Sediment in a Gravel-Bed River, *Catena*, *15*(1), 65-80, doi:10.1016/0341-8162(88)90017-3.

Landers, M. N., and T. W. Sturm (2013), Hysteresis in suspended sediment to turbidity relations due to changing particle size distributions, *Water Resources Research*, *49*(9), 5487-5500, doi:10.1002/wrcr.20394.

Le Pape, O., et al. (2013), Sources of organic matter for flatfish juveniles in coastal and estuarine nursery grounds: A meta-analysis for the common sole (Solea solea) in contrasted systems of Western Europe, *Journal of Sea Research*, *75*, 85-95, doi:10.1016/j.seares.2012.05.003.

Lefrançois, J., C. Grimaldi, C. Gascuel-Odoux, and N. Gilliet (2007), Suspended sediment and discharge relationships to identify bank degradation as a main sediment source on small agricultural catchments, *Hydrological Processes*, *21*(21), 2923-2933, doi:10.1002/hyp.6509.

Legout, C., J. Poulenard, J. Nemery, O. Navratil, T. Grangeon, O. Evrard, and M. Esteves (2013), Quantifying suspended sediment sources during runoff events in headwater catchments using spectrocolorimetry, *Journal of Soils and Sediments*, *13*(8), 1478-1492, doi:10.1007/s11368-013-0728-9.

Lloyd, C. E., J. E. Freer, P. J. Johnes, and A. L. Collins (2016), Using hysteresis analysis of high-resolution water quality monitoring data, including uncertainty, to infer controls on nutrient and sediment transfer in catchments, *Sci Total Environ*, *543*(Pt A), 388-404, doi:10.1016/j.scitotenv.2015.11.028.

Ludwig, W., and J. L. Probst (1998), River sediment discharge to the oceans; present-day controls and global budgets, *American Journal of Science*, *298*(4), 265-295, doi:10.2475/ajs.298.4.265.

Mano, V., J. Nemery, P. Belleudy, and A. Poirel (2009), Assessment of suspended sediment transport in four alpine watersheds (France): influence of the climatic regime, *Hydrological Processes*, *23*(5), 777-792, doi:10.1002/hyp.7178.

Mao, L., and R. Carrillo (2016), Temporal dynamics of suspended sediment transport in a glacierized Andean basin, *Geomorphology*, doi:10.1016/j.geomorph.2016.02.003.

Marden, M., G. Arnold, B. Gomez, and D. Rowan (2005), Pre- and post-reforestation gully development in Mangatu Forest, East Coast, North Island, New Zealand, *River Research and Applications*, *21*(7), 757-771, doi:10.1002/rra.882.

Marttila, H., and B. Kløve (2010), Dynamics of erosion and suspended sediment transport from drained peatland forestry, *Journal of Hydrology*, *388*(3-4), 414-425, doi:10.1016/j.jhydrol.2010.05.026.

Meybeck, M., L. Laroche, H. H. Dürr, and J. P. M. Syvitski (2003), Global variability of daily total suspended solids and their fluxes in rivers, *Global and Planetary Change*, *39*(1-2), 65-93, doi:10.1016/s0921-8181(03)00018-3.

Mooneyham, C., and K. Strom (2018), Deposition of Suspended Clay to Open and Sand-Filled Framework Gravel Beds in a Laboratory Flume, *Water Resources Research*, doi:10.1002/2017wr020748.

Navratil, O., M. Esteves, C. Legout, N. Gratiot, J. Nemery, S. Willmore, and T. Grangeon (2011), Global uncertainty analysis of suspended sediment monitoring using turbidimeter in a small mountainous river catchment, *Journal of Hydrology*, *398*(3-4), 246-259, doi:10.1016/j.jhydrol.2010.12.025.

Navratil, O., et al. (2012), Temporal variability of suspended sediment sources in an alpine catchment combining river/rainfall monitoring and sediment fingerprinting, *Earth Surface Processes and Landforms*, *37*(8), 828-846, doi:10.1002/esp.3201.

Navratil, O., C. Legout, D. Gateuille, M. Esteves, and F. Liebault (2010), Assessment of intermediate fine sediment storage in a braided river reach (southern French Prealps), *Hydrological Processes*, *24*(10), 1318-1332, doi:10.1002/hyp.7594.

Nistor, C. J., and M. Church (2005), Suspended sediment transport regime in a debris-flow gully on Vancouver Island, British Columbia, *Hydrological Processes*, *19*(4), 861-885, doi:10.1002/hyp.5549.

Orwin, J. F., and C. C. Smart (2004), Short-term spatial and temporal patterns of suspended sediment transfer in proglacial channels, Small River Glacier, Canada, *Hydrological Processes*, *18*(9), 1521-1542, doi:10.1002/hyp.1402.

Park, J., and J. R. Hunt (2017), Coupling fine particle and bedload transport in gravel-bedded streams, *Journal of Hydrology*, *552*, 532-543, doi:10.1016/j.jhydrol.2017.07.023.

Parsons, A. J., L. Bracken, R. E. Poeppl, J. Wainwright, and S. D. Keesstra (2015), Introduction to special issue on connectivity in water and sediment dynamics, *Earth Surface Processes and Landforms*, *40*(9), 1275-1277, doi:10.1002/esp.3714.

Picouet, C., B. Hingray, and J. C. Olivry (2009), Modelling the suspended sediment dynamics of a large tropical river: the Upper Niger river basin at Banankoro, *Hydrological Processes*, *23*(22), 3193-3200, doi:10.1002/hyp.7398.

Piqué, G., J. A. López-Tarazón, and R. J. Batalla (2014), Variability of in-channel sediment storage in a river draining highly erodible areas (the Isábena, Ebro Basin), *Journal of Soils and Sediments*, *14*(12), 2031-2044, doi:10.1007/s11368-014-0957-6.

Roux, C., A. Alber, M. Bertrand, L. Vaudor, and H. Piégay (2015), “FluvialCorridor”: A new ArcGIS toolbox package for multiscale riverscape exploration, *Geomorphology*, *242*, 29-37, doi:10.1016/j.geomorph.2014.04.018.

Smith, H. G., and D. Dragovich (2009), Interpreting sediment delivery processes using suspended sediment-discharge hysteresis patterns from nested upland catchments, south-eastern Australia, *Hydrological Processes*, *23*(17), 2415-2426, doi:10.1002/hyp.7357.

Soler, M., J. Latron, and F. Gallart (2008), Relationships between suspended sediment concentrations and discharge in two small research basins in a mountainous Mediterranean area (Vallcebre, Eastern Pyrenees), *Geomorphology*, *98*(1-2), 143-152, doi:10.1016/j.geomorph.2007.02.032.

Sun, L., M. Yan, Q. Cai, and H. Fang (2016), Suspended sediment dynamics at different time scales in the Loushui River, south-central China, *Catena*, *136*, 152-161, doi:10.1016/j.catena.2015.02.014.

Tananaev, N. I. (2012), Hysteresis effect in the seasonal variations in the relationship between water discharge and suspended load in rivers of permafrost zone in Siberia and Far East, *Water Resources*, *39*(6), 648-656, doi:10.1134/s0097807812060073.

Tananaev, N. I. (2015), Hysteresis effects of suspended sediment transport in relation to geomorphic conditions and dominant sediment sources in medium and large rivers of the Russian Arctic, *Hydrology Research*, *46*(2), doi:10.2166/nh.2013.199.

Trustrum, N. A., and P. R. Stephens (1981), Selection of hill-country pasture measurement sites by interpretation of sequential aerial photographs, *New Zealand Journal of Experimental Agriculture*, *9*(1), 31-34, doi:10.1080/03015521.1981.10427799.

Vaughan, A. A., P. Belmont, C. P. Hawkins, and P. Wilcock (2017), Near-Channel Versus Watershed Controls on Sediment Rating Curves, *Journal of Geophysical Research: Earth Surface*, *122*(10), 1901-1923, doi:10.1002/2016jf004180.

Vercruysse, K., R. C. Grabowski, and R. J. Rickson (2017), Suspended sediment transport dynamics in rivers: Multi-scale drivers of temporal variation, *Earth-Science Reviews*, *166*, 38-52, doi:10.1016/j.earscirev.2016.12.016.

Vrieling, A. (2006), Satellite remote sensing for water erosion assessment: A review, *Catena*, *65*(1), 2-18, doi:10.1016/j.catena.2005.10.005.

Walling, D. E., P. N. Owens, J. Cartera, G. J. L. Leeks, S. Lewis, A. A. Meharg, and J. Wright (2003), Storage of sediment-associated nutrients and contaminants in river channel and floodplain systems, *Applied Geochemistry*, *18*(2), 195-220, doi:10.1016/S0883-2927(02)00121-X.

Williams, G. P. (1989), Sediment concentration versus water discharge during single hydrologic events in rivers, *Journal of Hydrology*, *111*, 89-106, doi:10.1016/0022-1694(89)90254-0.

Wohl, E. (2017), Connectivity in rivers, *Progress in Physical Geography*, *41*(3), 345-362, doi:10.1177/0309133317714972.

Zuecco, G., D. Penna, M. Borga, and H. J. van Meerveld (2016), A versatile index to characterize hysteresis between hydrological variables at the runoff event timescale, *Hydrological Processes*, *30*(9), 1449-1466, doi:10.1002/hyp.10681.

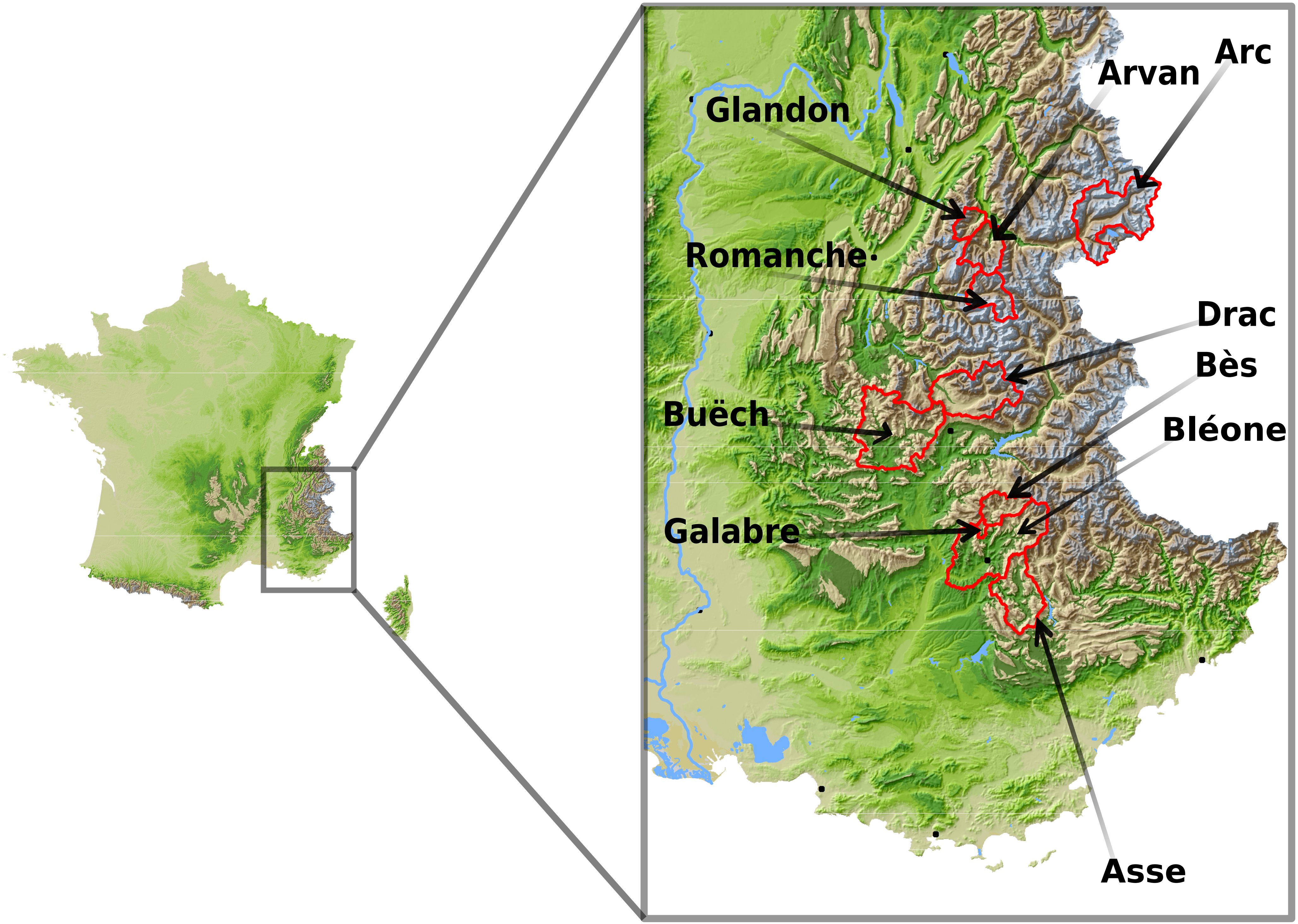

Arc
Arvan
Glandon
Romanche
Drac
Bès
Buëch
Bléone
Galabre
Asse

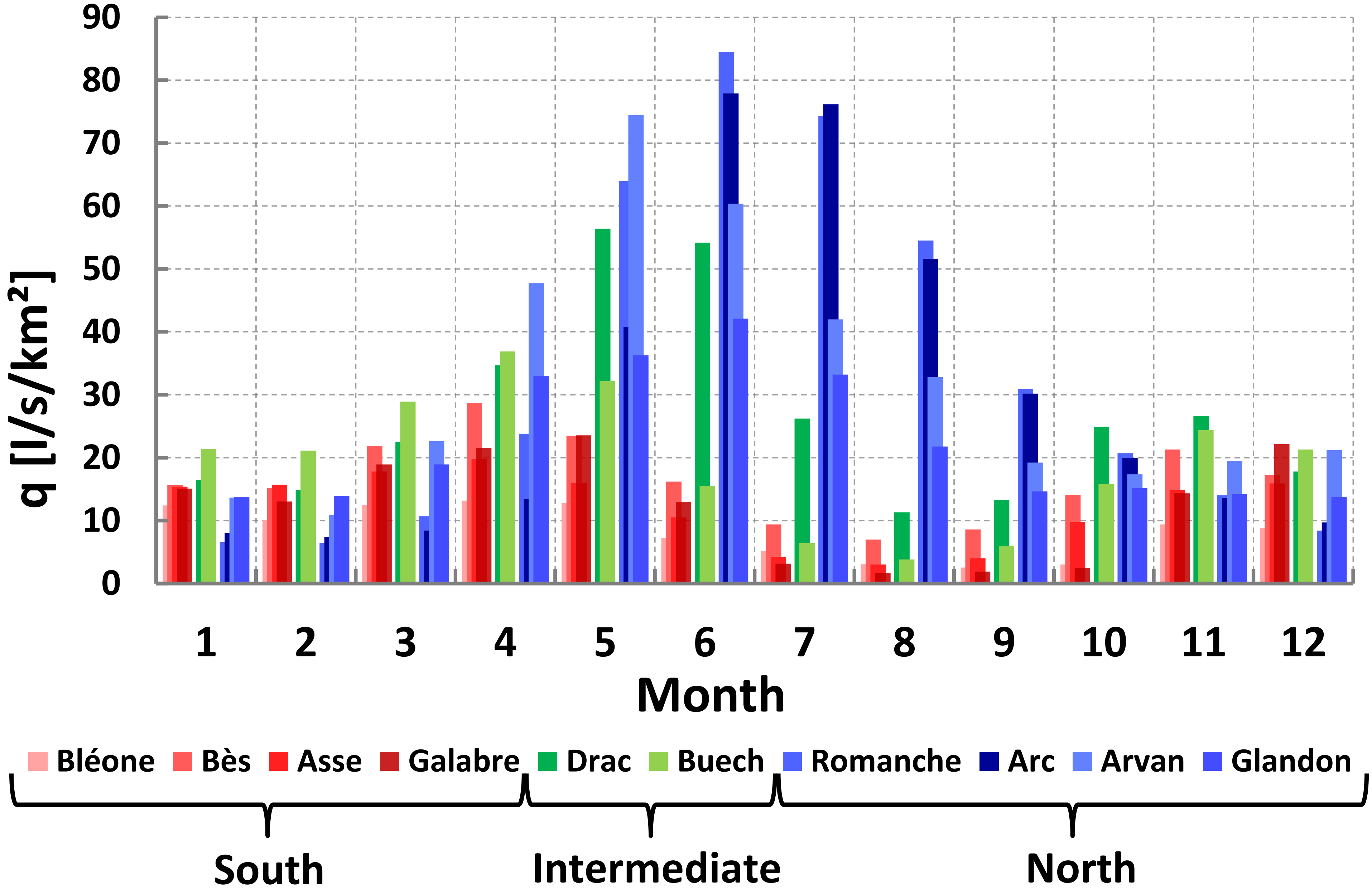

q [l/s/km²]
90
80
70
60
50
40
30
20
10
0
1
2
3
4
5
6
7
8
9
10
11
12
Month
Bléone
Bès
Asse
Galabre
Drac
Buech
Romanche
Arc
Arvan
Glandon
South
Intermediate
North

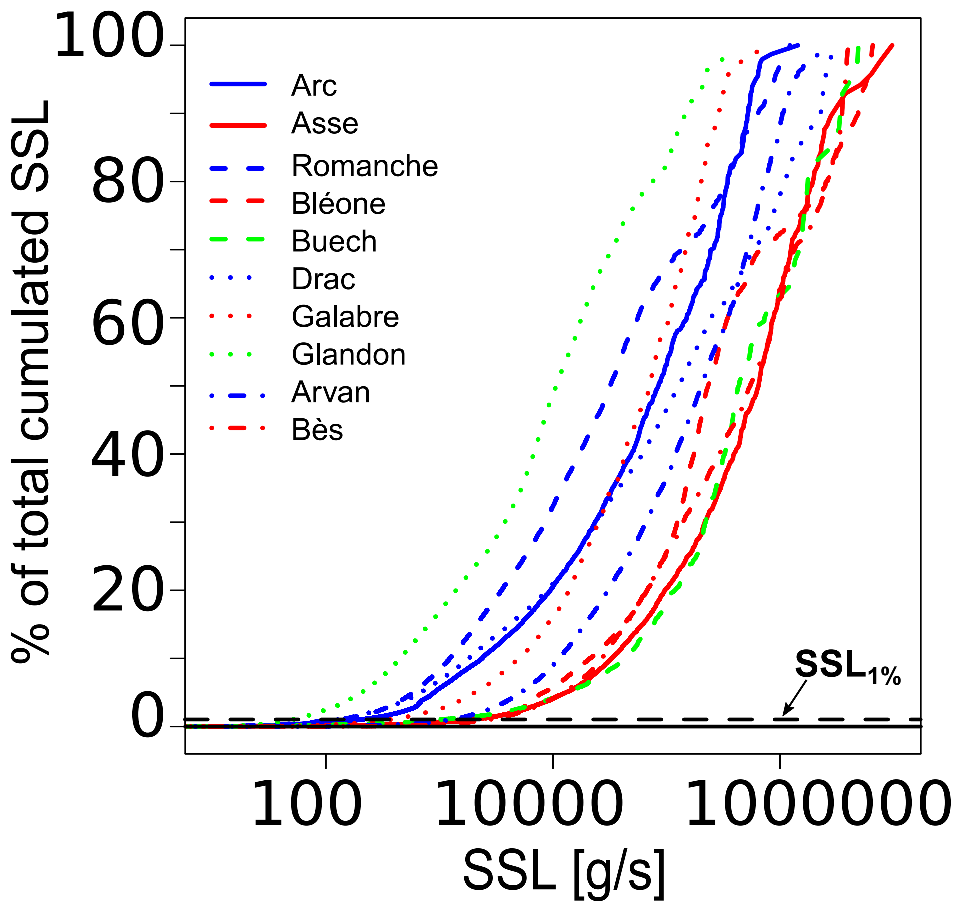
100
80
60
40
20
0
% of total cumulated SSL
Arc
Asse
Romanche
Bléone
Buech
Drac
Galabre
Glandon
Arvan
Bès
SSL1%
100
10000
1000000
SSL [g/s]

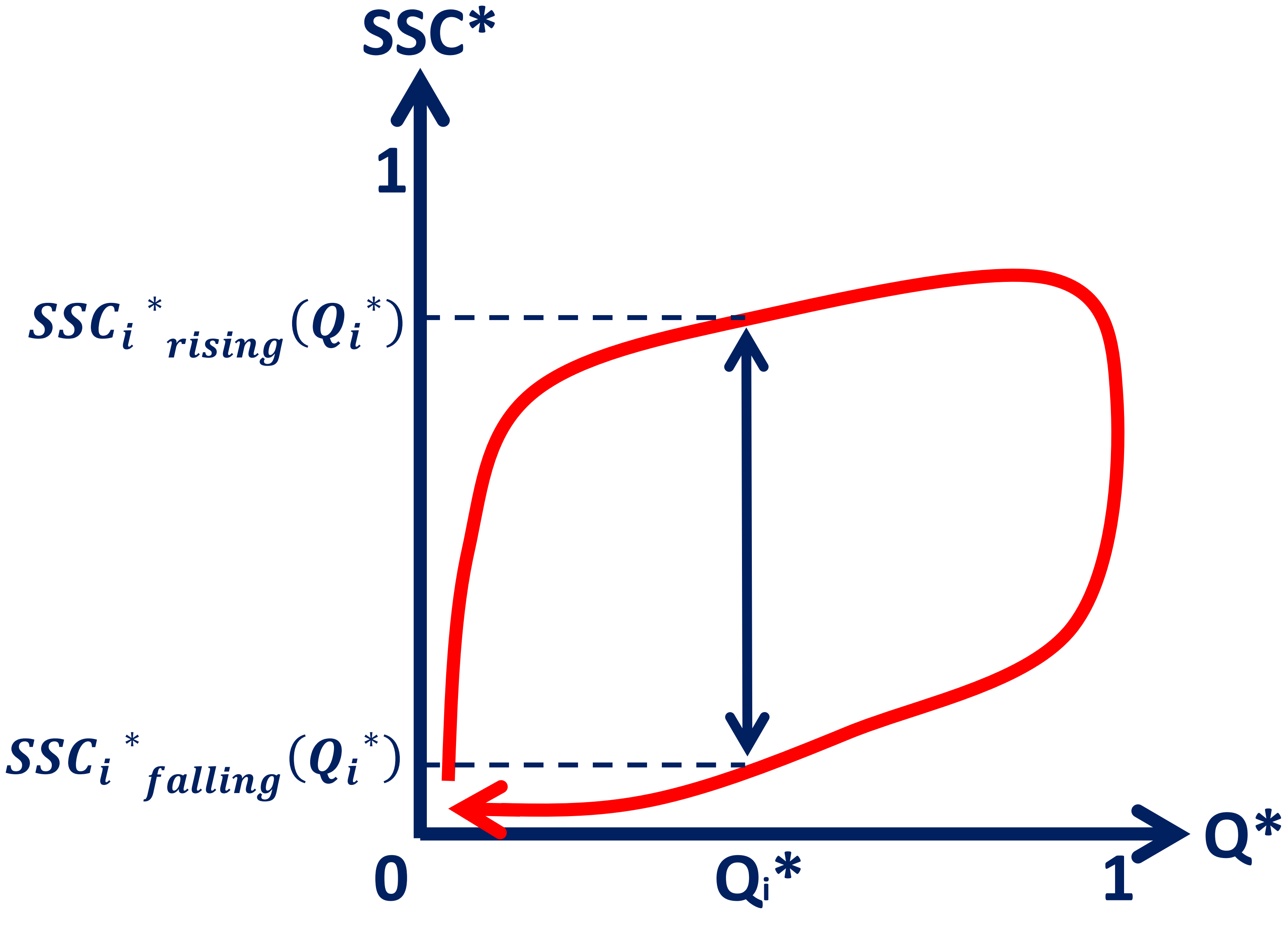
SSC*
1
$SSC_i{}^*{}_{rising}(Q_i{}^*)$
$SSC_i{}^*{}_{falling}(Q_i{}^*)$
Q*
0
Q_i*
1

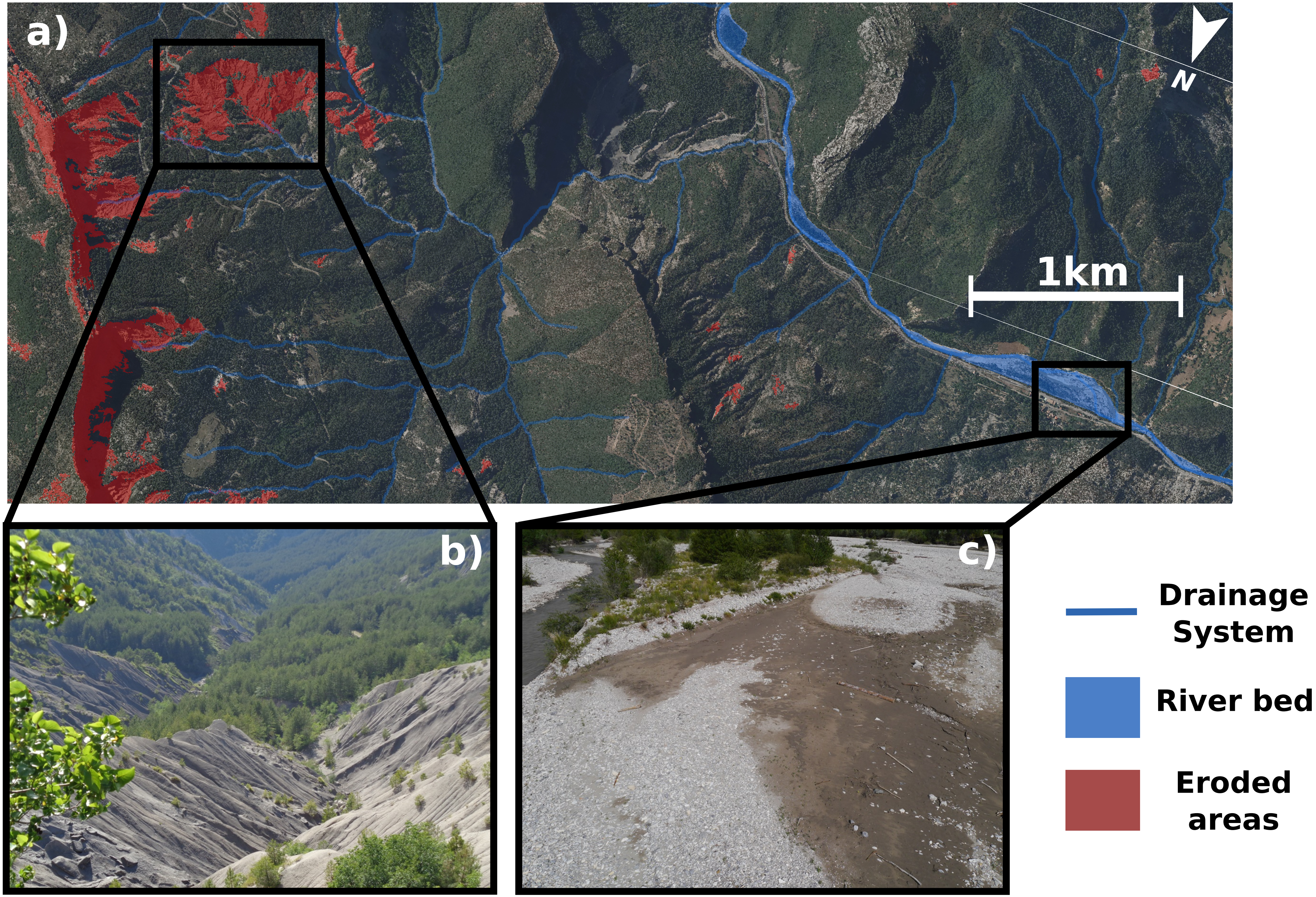
a)
N
1km
b)
c)
Drainage System
River bed
Eroded areas

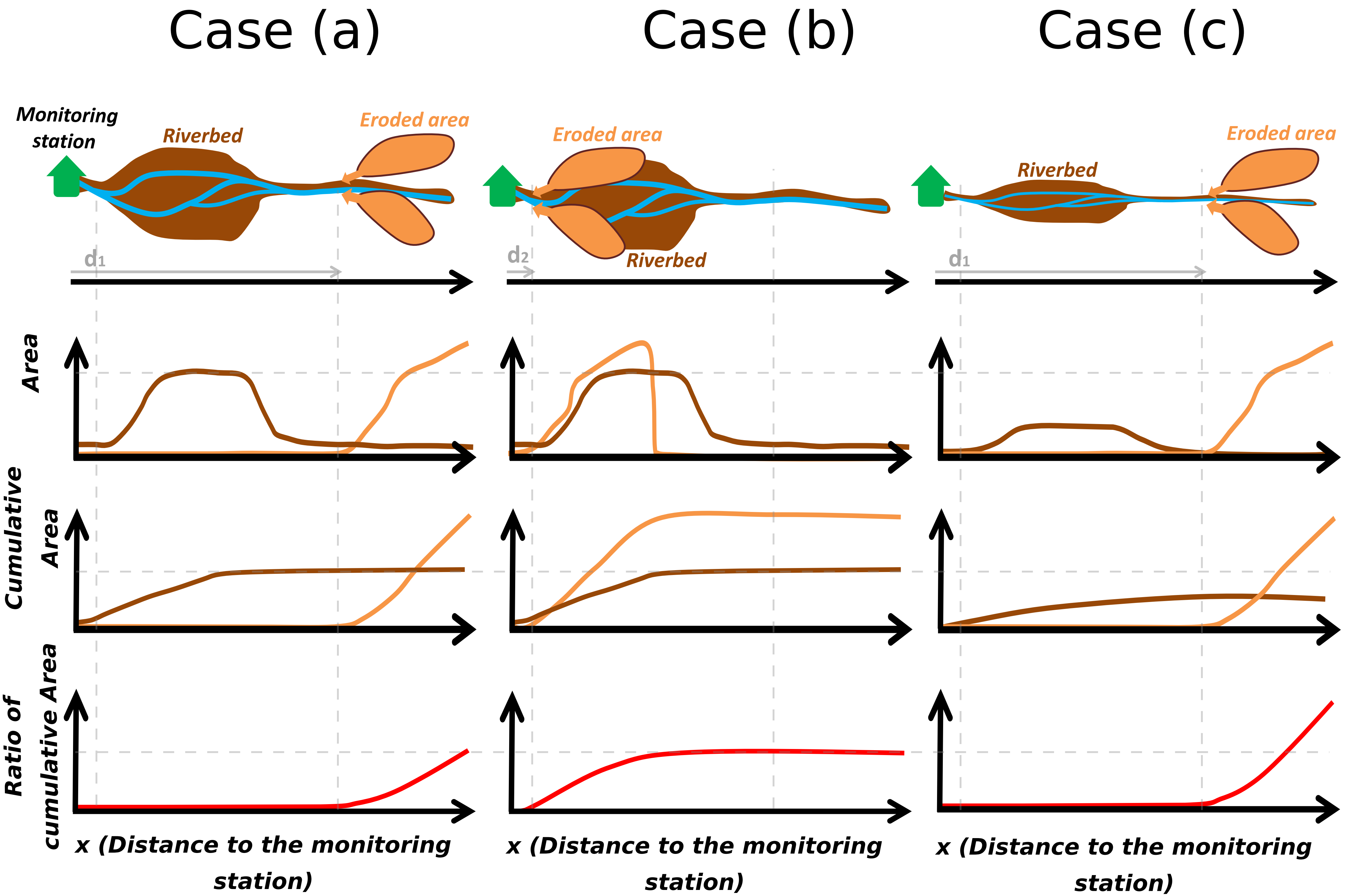

Case (a)
Case (b)
Case (c)
Monitoring station
Riverbed
Eroded area
Eroded area
Riverbed
Eroded area
Riverbed
d1
d2
d1
Area
Cumulative Area
Ratio of cumulative Area
x (Distance to the monitoring station)
x (Distance to the monitoring station)
x (Distance to the monitoring station)

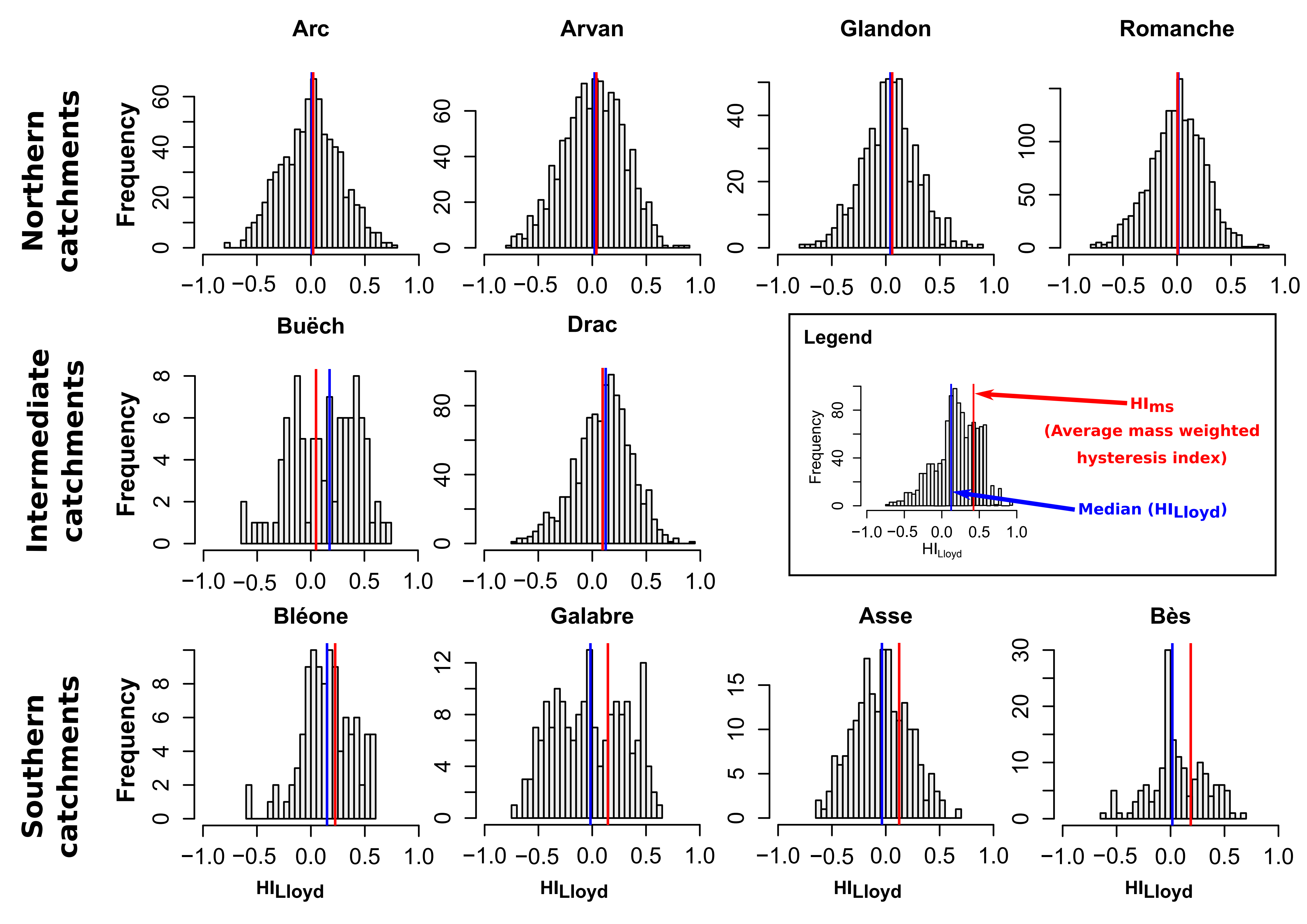

Arc
Arvan
Glandon
Romanche
Northern catchments
Frequency
Buëch
Drac
Intermediate catchments
Legend
HIms
(Average mass weighted hysteresis index)
Median (HILloyd)
HILloyd
Bléone
Galabre
Asse
Bès
Southern catchments
HILloyd

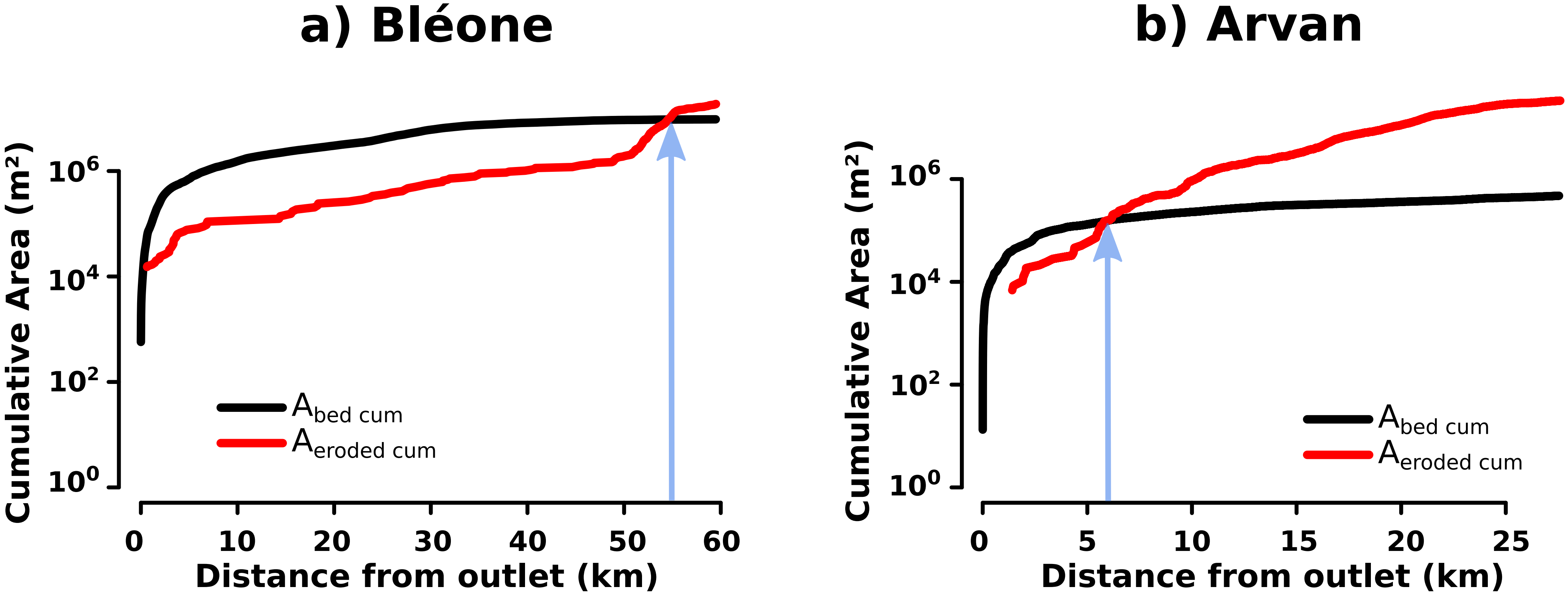

a) Bléone
b) Arvan
Cumulative Area (m²)
10⁶
10⁴
10²
10⁰
A bed cum
A eroded cum
0
10
20
30
40
50
60
5
15
25
Distance from outlet (km)

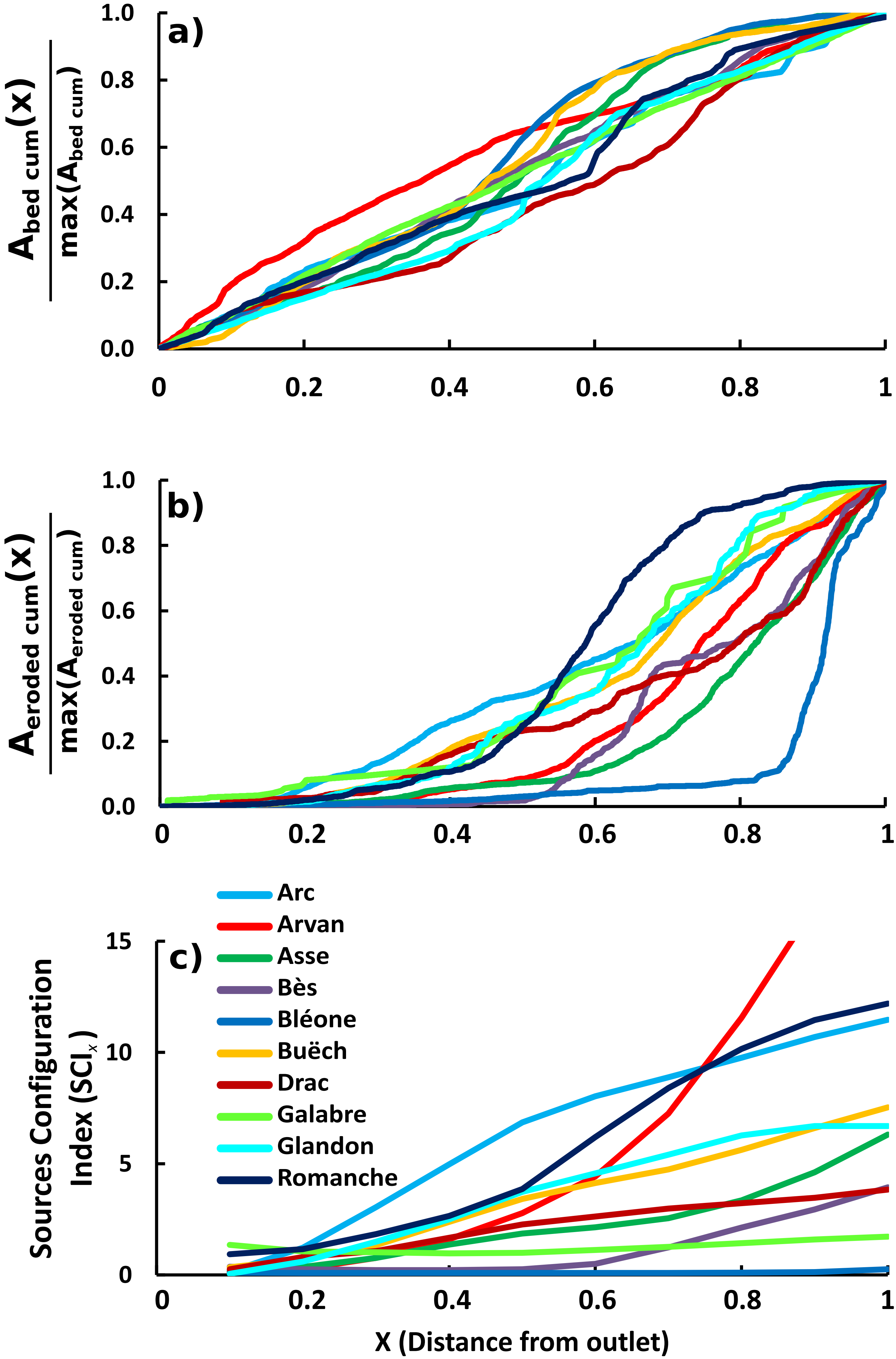

a)
b)
c)
$\frac{A_{bed\ cum}(x)}{max(A_{bed\ cum})}$
$\frac{A_{eroded\ cum}(x)}{max(A_{eroded\ cum})}$
Sources Configuration Index (SCI_x)
X (Distance from outlet)
0.0
0.2
0.4
0.6
0.8
1.0
0
5
10
15
0
0.2
0.4
0.6
0.8
1
Arc
Arvan
Asse
Bès
Bléone
Buëch
Drac
Galabre
Glandon
Romanche

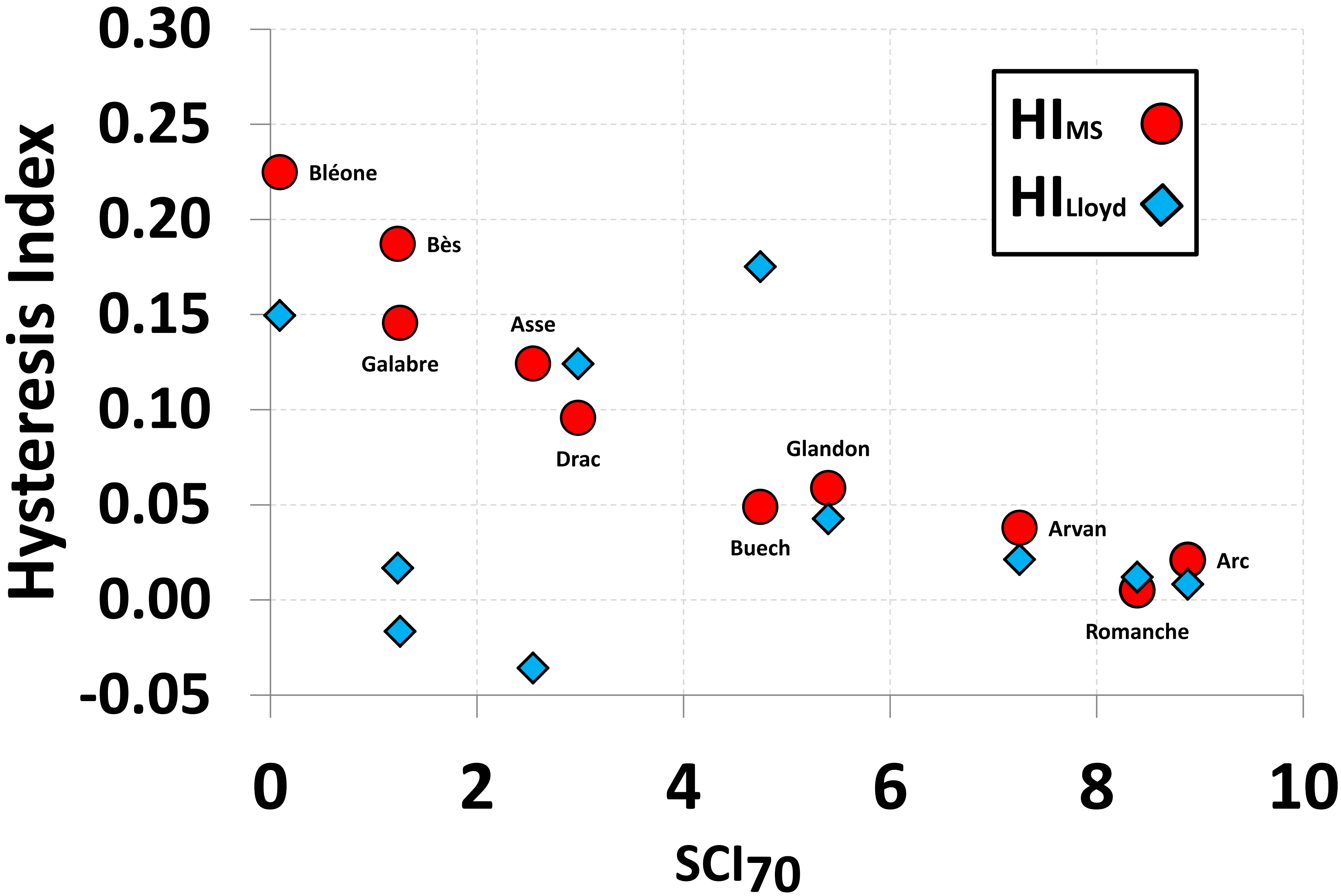

Hysteresis Index
0.30
0.25
0.20
0.15
0.10
0.05
0.00
-0.05
0
2
4
6
8
10
SCI70
HIMS
HILloyd
Bléone
Bès
Galabre
Asse
Drac
Glandon
Buech
Arvan
Arc
Romanche

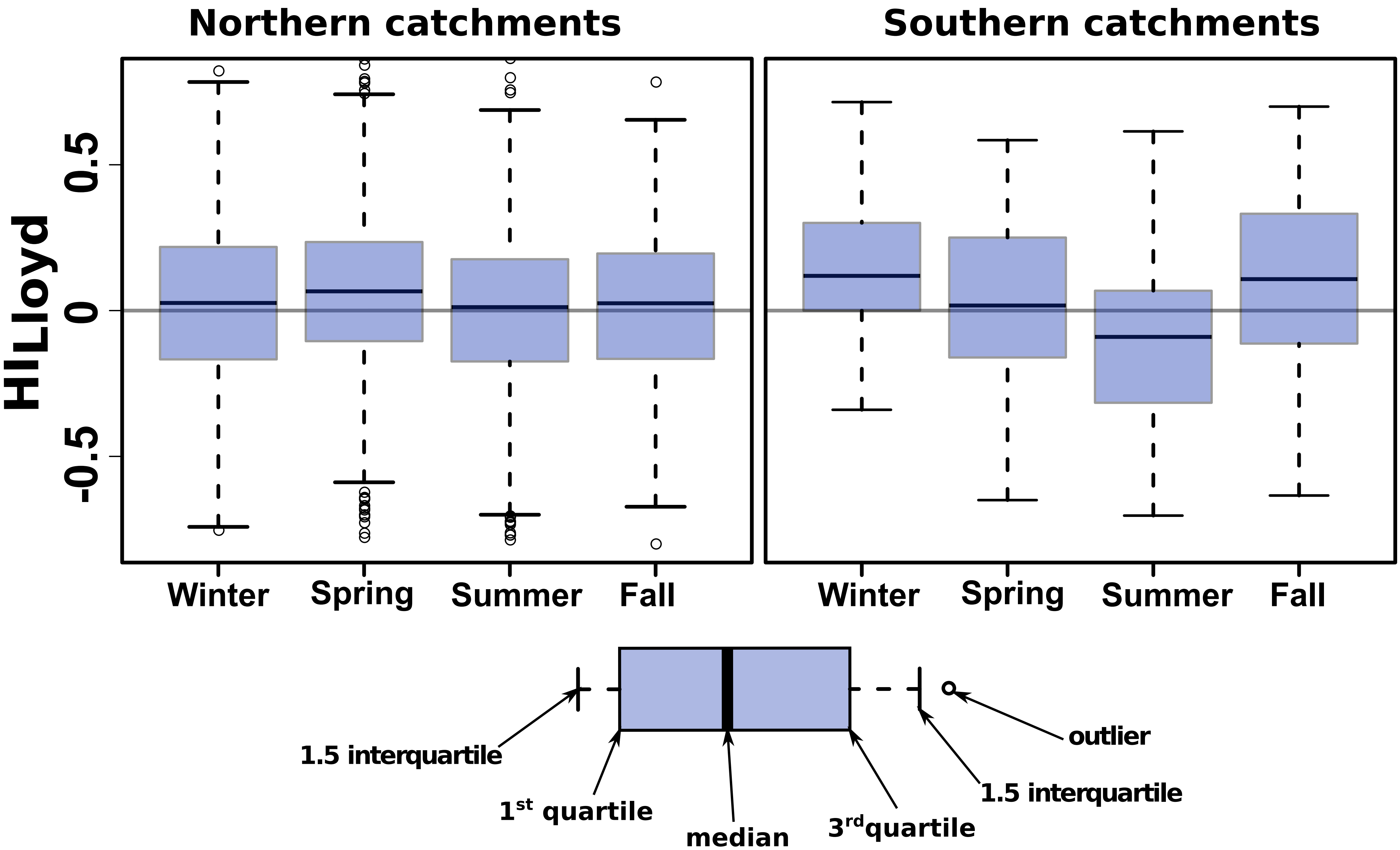

Northern catchments
Southern catchments
HILloyd
0.5
0
-0.5
Winter
Spring
Summer
Fall
Winter
Spring
Summer
Fall
1.5 interquartile
1st quartile
median
3rdquartile
1.5 interquartile
outlier

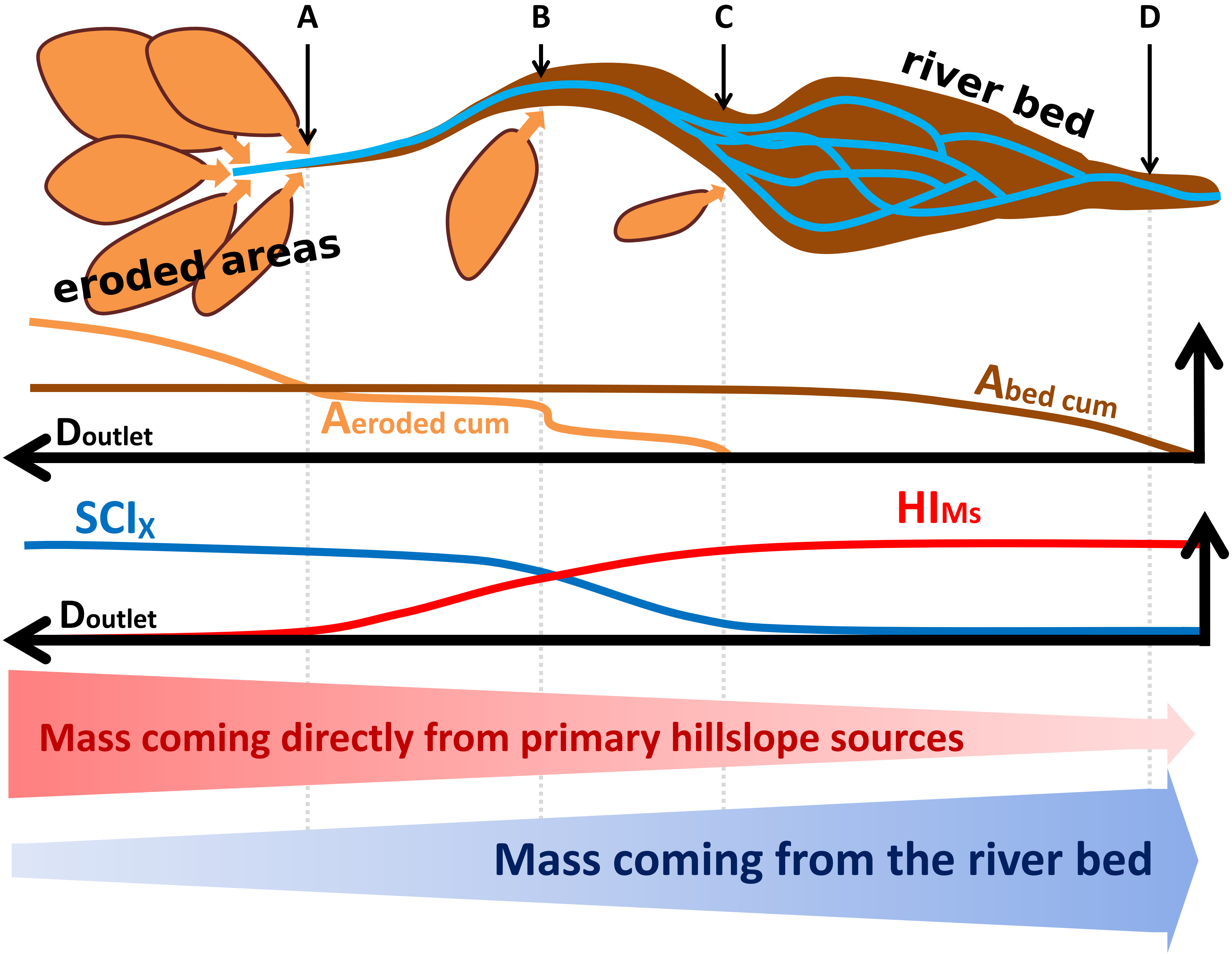

A
B
C
D
river bed
eroded areas
Abed cum
Aeroded cum
Doutlet
SCIx
HIMs
Doutlet
Mass coming directly from primary hillslope sources
Mass coming from the river bed

Basins names	A [km²]	No [%]	Fo [%]	Gl [%]	SCR [%]	HR [%]	RR [%]	W_{10} [m]	S_{10} [%]	q [l/s/km²]	Period
Arc	635	49	11	9	0	64	36	33	1.12	30	2012 - 2016
Arvan	220	24	18	2	38	61	1	22	5.92	32	2011 - 2015
Asse	375	10	41	0	9	70	21	28	0.87	12	2011 - 2016
Bès	165	14	43	0	42	46	11	20	2.57	17	2007 - 2013
Bléone	896	14	41	0	19	68	11	162	0.82	8	2007 - 2009
Buech	723	12	47	0	83	1	12	118	0.81	19	2015 - 2017
Drac	510	35	20	0	32	34	18	60	1.01	27	2007 - 2016
Galabre	22	19	11	0	39	61	0	8	8.86	13	2007 - 2013
Glandon	110	31	28	2	0	57	43	8	5.80	23	2011 - 2016
Romanche	230	51	4	12	25	33	42	14	4.17	33	2007 - 2016

Table 1: Main catchment characteristics. Catchment size (A), no/low vegetation cover (No), forest cover (Fo), glacier cover (Gl), soft coherent rocks (SCR), heterogeneous rocks (HR), resistant rocks (RR), mean annual specific discharge (q), median active channel width calculated for the first 10 km (W10), mean slope of the river bed calculated for approximately the first 10 km (S10).

River	$SSL_{1\%}$ [g/s]	$SSC_{1\%}$ [mg/l]	t_{exceed} [h]	number of event
Arc	199	23	8	758
Arvan	1252	330	8	1048
Asse	1877	311	8	217
Bès	2677	868	8	155
Bleone	2000	181	12	104
Buech	960	104	8	94
Drac	125	14	12	1076
Galabre	360	1215	4	179
Glandon	50	21	8	561
Romanche	125	26	6	1656

Table 2: Runoff event characteristics. (SSL1%) corresponds to the threshold of SSL below which 1% of the cumulated suspended sediment fluxes were transported, (SSC1%) corresponds to the threshold of SSC below which 1% of the cumulated suspended sediment fluxes were transported, texceed corresponds to the minimum time step for which a valid SSL peak should exceed all following and preceding values.

	Mass transported			Number of events			Indexes		
River	Ms_{cl} [%]	Ms_{ccl} [%]	$Ms_{no/complex}$ [%]	Nb_{cl} [%]	Nb_{ccl} [%]	$Nb_{no/complex}$ [%]	median(HI_{Lloyd})	Sd(HI_{Lloyd})	HI_{Ms}
Arc	26	32	42	30	32	37	0.01	0.27	0.02
Arvan	34	28	38	34	30	36	0.02	0.28	0.04
Asse	58	11	31	23	31	47	-0.04	0.25	0.12
Bès	58	4	38	38	15	47	0.02	0.26	0.19
Bleone	84	2	14	60	11	30	0.15	0.24	0.22
Buech	41	31	28	62	19	19	0.18	0.31	0.05
Drac	41	24	35	43	16	41	0.12	0.26	0.10
Galabre	53	21	26	37	41	22	-0.02	0.33	0.15
Glandon	44	22	34	38	28	34	0.04	0.25	0.06
Romanche	25	28	47	28	28	43	0.01	0.25	0.01

Table 3: Results of hysteresis analysis between SSC and Q. The percentage of the mass transported with a given hysteresis shape (Ms), the percentage of events with a given shape (Nb), and the mean, standard deviation (sd) of the Lloyd hysteresis index (HI_{Lloyd}) were calculated as well as the average mass weighted hysteresis index (HI_{Ms}). cl : clockwise hysteresis, ccl : counterclockwise hysteresis, no/complex : no or complex hysteresis.

General catchment characteristics			River bed area configuration			Eroded area configuration			River bed and eroded area configuration		
	HI_{MS}	HI_{Lloyd} median		HI_{MS}	HI_{Lloyd} median		HI_{MS}	HI_{Lloyd} median		HI_{MS}	HI_{Lloyd} median
S_{10}	-0.19	**-0.44**	BAI_{10}	0.10	**-0.45**	EAI_{10}	0.32	0.02	SCI_{10}	-0.01	-0.35
W_{10}	0.12	**0.56**	BAI_{30}	0.13	**-0.13**	EAI_{30}	**-0.26**	-0.08	SCI_{30}	**-0.78**	-0.14
A	-0.05	**0.47**	BAI_{50}	0.38	-0.04	EAI_{50}	**-0.43**	-0.14	SCI_{50}	**-0.94**	-0.07
No	**-0.63**	-0.08	BAI_{70}	0.37	0.25	EAI_{70}	**-0.71**	-0.22	SCI_{70}	**-0.98**	-0.13
Fo	**0.54**	**0.49**	BAI_{90}	0.35	0.22	EAI_{90}	**-0.71**	-0.25	SCI_{90}	**-0.93**	-0.10

Table 4: Spearman correlation coefficients between hysteresis indexes considering the frequency of event with a given hysteresis (median value of the Lloyd index, HI_{Lloyd}) or the mass transported with a given hysteresis (average mass weighted hysteresis index, HI_{Ms}) and catchment characteristics: S_{10} is the mean river bed slope calculated for the first 10 km, W_{10} is the median active width calculated for the first 10 km, A is the catchment size, No is the percentage of the catchment having no or low vegetation cover, and Fo is the forest cover, BAI_x is the mean ratio of cumulated river bed area over total cumulated river bed area considering a length x upstream of the station, EAI_x is the mean ratio of cumulated eroded area over total cumulated eroded area considering a length x upstream of the station and SCI_x is the mean ratio of cumulated eroded area over cumulated bed area considering a length x upstream of the station. Bold values are significant with a confidence interval of 95% (p_{value}<0.01).